Early dissemination highly enhances liver metastasis development during intestinal tumorigenesis

Zeinab Homayed, Guillaume Belthier, Tinhinan Lahlou, Laia Bassaganyas, Emmanuelle Sidot, Pierre Giroux, Jennifer Series, Lucile Bansard, François Gerbe, Chenchen Pan, et al.

Cancer Cell

Early dissemination highly enhances liver metastasis development during intestinal tumorigenesis

--Manuscript Draft--

Manuscript Number:	
Full Title:	Early dissemination highly enhances liver metastasis development during intestinal tumorigenesis
Article Type:	Research Article
Keywords:	Early dissemination, pre metastatic niche, intestinal tumorigenesis and systemic factors
Corresponding Author:	Julie Pannequin Institute of Functional Genomics Montpellier, FRANCE
First Author:	Zeinab Homayed
Order of Authors:	Zeinab Homayed
	Guillaume Belthier
	Tinhinan Lahlou
	Laia Bassaganyas
	Emmanuelle Sidot
	Pierre Giroux
	Jennifer Series
	Lucile Bansard
	François Gerbe
	Chenchen Pan
	Moritz Newger
	Jean Francois Bourgaux
	Julie Guillermet-Guibert
	Matthieu Lacroix
	Laurent Le Cam
	Silvia Fre
	Rachel Ridgway
	Owen Sansom
	Ali Erturk
	Philippe Jay
	Daniel Häußler
	Achim Krüger
	Zena Werb
	Andrei Turtoi
	Damien Gregoire
	Frederic Lagarrigue
	Caroline Bonnans
	Julie Pannequin

Abstract:	The ability of yet benign tumor cells to disseminate from the primary tumor before transforming to their full metastatic potential has recently received increasing attention. So far, the existence of such function of cells at early benign stages of intestinal tumorigenesis could not be demonstrated. Here, we introduced and characterized a genetic mouse model with specific tamoxifen-driven induction of tumorigenesis in intestinal tdTomato expressing cells. This model enabled us, already at the adenoma stage, to detect the sparse but obvious presence of intestinal disseminated cells in the liver. In parallel, an elevated plasma level of TIMP1, most prominently, as well as TNF-α, SDF-1, CXCL2, and M-CSF was detected, a pattern, which was also observed in blood of patients with benign intestinal polyps. In the liver, the presence of early disseminated cells, in synergy with the detected systemic factors, was accompanied by severe infiltration of myeloid cells including macrophages and neutrophils. This enrichment facilitated metastatic growth in this organ when challenged with carcinoma cell inoculation. This study expands the concept of the impact of early disseminated intestinal cells in synergy with circulating factors on the creation of a pre-metastatic niche to promote distant metastases.
Suggested Reviewers:	Julio Aguirre Ghiso julio.aguirre-ghiso@einsteinmed.edu Pr Aguirre is one of the key leader of opinion in the field of early dissemination
	Christoph Klein christoph.klein@ukr.de Pr Klein is one of the main pionner is the field of early dissemination
	Christina Curtis cncurtis@stanford.edu Dr Curtis has published in 2019 the first evidence from an elegant computational study that early dissemination could occur in colorectal cancer
Opposed Reviewers:	Klaus Pantel University Medical Center Hamburg-Eppendorf Department of Tumor Biology Conflict of interest
	Catherine Alix-Panabieres University Hospital Centre Montpellier Conflict of interest
	Jean-Yves Pierga Institute Curie conflict of interest
Additional Information:	
Question	**Response**
Original Code Does this manuscript report original code?	No
Standardized datasets A list of datatypes considered standardized under Cell Press policy is available here. Does this manuscript report new standardized datasets?	Yes
Reviewers must have anonymous access to these standardized datasets that is free-of-cost. Please provide dataset locations and instructions for access here. If applicable, include accession numbers	We are currently preparing the raw data for GEO submission. The accession link will be provided by the time of the manuscript revision.

and reviewer tokens. Please consult these Author's guides for more information: "Standardized datatypes, datatype-specific repositories, and general-purpose repositories recommended by Cell Press" and "How standardized datasets and original code accompany Cell Press manuscripts from submission through publication" or email us at cancer@cell.com. as follow-up to "**Standardized datasets** A list of datatypes considered standardized under Cell Press policy is available here. Does this manuscript report new standardized datasets? "	
Clinical Trials Does your manuscript report clinical trial results?	Yes
Has the study been registered at ClinicalTrials.gov (or an equivalent database)? as follow-up to "**Clinical Trials** Does your manuscript report clinical trial results?"	Yes
Please provide the registration number here. as follow-up to "Has the study been registered at ClinicalTrials.gov (or an equivalent database)? "	NCT05648240

Dear Editor,

Based on your wish to discover the whole story during the presubmission process, we would like to submit manuscript entitled "**Early dissemination highly enhances liver metastasis development during intestinal tumorigenesis**" as an original paper to Cancer Cell.

In the classical model of metastasis, the dissemination of tumor cells occurs at late stages of cancer disease. However, recent studies have demonstrated that tumor cells can spread to distant organs at much earlier stages than previously believed. Recently, an elegant computational study from patient samples has strongly suggested that early dissemination could also occur in colorectal cancer. However, despite the prevalence and lethality of colorectal cancer, no functional study on early tumor dissemination had been yet performed.

In this study, we have filled this void by introducing and characterizing an inducible mouse model that enables the tracking of cellular dissemination during the onset of intestinal tumorigenesis.

Using this model, we track rare **intestinal cells disseminating into liver**, which is the main organ for metastasis development in man. This early dissemination induces liver remodeling, including a drastic myeloid cell enrichment. By add back experiments we show that early-disseminated tumor cells alone can remodel the liver when they are injected in mice.

We also show that liver remodeling, induced **by early disseminated cells in synergy with cytokines**, **greatly facilitates late metastatic cell colonization**

Importantly we confirm these results in various complementary mouse models.

Importantly also, some **myeloid cell-associated cytokines** are more present in the plasma of mice developing adenomas and in **the plasma of patients diagnosed with intestinal polyps.**

Overall, this is a significant breakthrough in the field of tumor dissemination in colorectal cancer, for which metastasis is invariably the last fatal stage of the disease.

We thank you for your consideration.

Best regards,

Julie Pannequin

Graphical Abstract

Click here to access/download;Graphical Abstract;Homayed_GA.tif

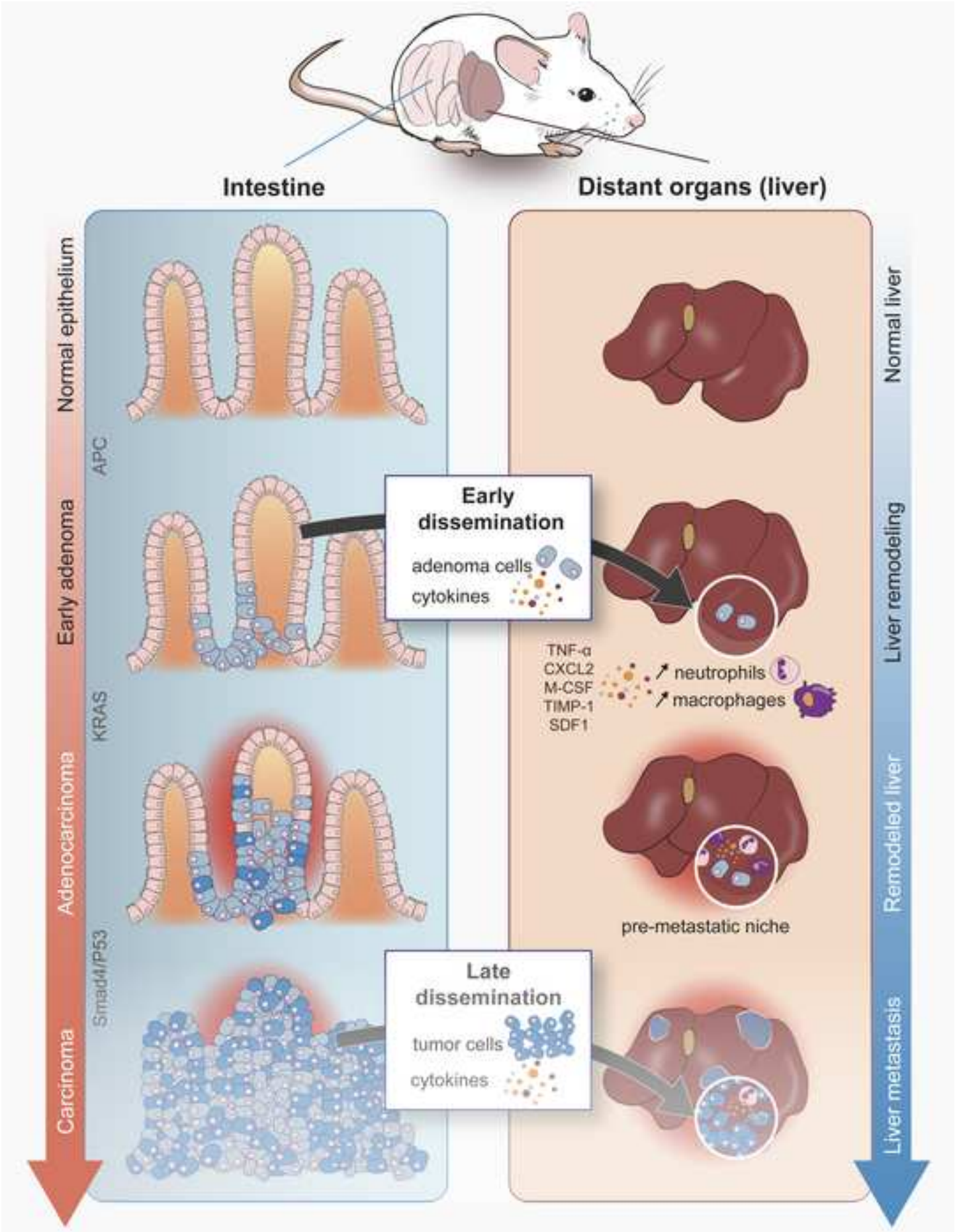

Early dissemination highly enhances liver metastasis development during intestinal tumorigenesis

Homayed Z[1], Belthier G*[1], Lahlou T*[1], Bassaganyas L[1], Sidot E[1], Giroux P[1], Series J[2], Bouclier C[1], Bansard L[1], Gerbe F[1], Pan C[3], Newger M[3], Bourgaux JF[4], Guillermet-Guibert J[5], Lacroix M[6], Le Cam L[6], Fre S[7], Ridgway R[8], Sansom O[8], Erturk A[3], Jay P[1], Häußler D[9], Krüger A[9], Werb Z[†,10], Turtoi A[6], Gregoire D[11], Lagarrigue F[2], Bonnans C[1-10], and Pannequin J[1#]

[#] Corresponding author

[†] Deceased

* Authors have equally contributed

[1] Institut de Génomique Fonctionnelle, Univ. Montpellier, CNRS, INSERM, Montpellier, France

[2] Institut de Pharmacologie et Biologie Structurale, Université de Toulouse, Centre National de la Recherche Scientifique, Université Paul Sabatier, Toulouse, France.

[3] Institute for Tissue Engineering and Regenerative Medicine (iTERM), Helmholtz Center, Neuherberg, Munich, Germany

[4] Service d'Hépato-Gastroentérologie, CHU Carémeau, Nîmes, France

[5] INSERM, CNRS, Université Paul Sabatier, U1037, CRCT, Toulouse, France.

[6] IRCM, INSERM U1194, Univ. Montpellier, Institut régional du Cancer de Montpellier, Montpellier, France.

[7] Institut Curie, Laboratory of Genetics and Developmental Biology, PSL Research University, INSERM U934, CNRS UMR3215, Paris, France.

[8] Cancer Research UK Beatson Institute, Glasgow, UK; Institute of Cancer Sciences, University of Glasgow, Garscube Estate, Glasgow, UK.

[9] School of Medicine, Institute of Experimental Oncology and Therapy Research, Technical University of Munich, Munich, Germany

[10] Department of Anatomy, University of California, San Francisco, San Francisco CA 94143, USA

[11]Institut de Génétique Moléculaire de Montpellier, Univ. Montpellier, CNRS, Montpellier, France

Keywords

Early dissemination, pre metastatic niche, intestinal tumorigenesis and systemic factors.

Summary

The ability of yet benign tumor cells to disseminate from the primary tumor before transforming to their full metastatic potential has recently received increasing attention. So far, the existence of such function of cells at early benign stages of intestinal tumorigenesis could not be demonstrated. Here, we introduced and characterized a genetic mouse model with specific tamoxifen-driven induction of tumorigenesis in intestinal tdTomato expressing cells. This model enabled us, already at the adenoma stage, to detect the sparse but obvious presence of intestinal disseminated cells in the liver. In parallel, an elevated plasma level of TIMP1, most prominently, as well as TNF-α, SDF-1, CXCL2, and M-CSF was detected, a pattern, which was also observed in blood of patients with benign intestinal polyps.

In the liver, the presence of early disseminated cells, in synergy with the detected systemic factors, was accompanied by severe infiltration of myeloid cells including macrophages and neutrophils. This enrichment facilitated metastatic growth in this organ when challenged with carcinoma cell inoculation.

This study expands the concept of the impact of early disseminated intestinal cells in synergy with circulating factors on the creation of a pre-metastatic niche to promote distant metastases.

INTRODUCTION

According to the World Health Organization (WHO), around 10 million people die each year from metastatic cancer[1].

Despite a century of studies, the process of tumor dissemination remains poorly described. In the classical model of metastasis, the dissemination of tumor cells occurs at a late stage of cancer disease, when the tumor cells have gained their full malignant potential; after the primary tumor has grown and acquired mutations, the malignant tumor cells can invade the local tissue, enter the blood or lymphatic vessels, and colonize distant organs.

However, there is growing evidence in some cancers that tumor cells spread to distant organs much earlier than previously believed. For example, early dissemination has been described in melanoma, pancreas, lung, gastric and breast cancer using elegant mouse models and validated on patient samples[2–7].

Considering the significant incidence and mortality rates of colorectal cancer (CRC) worldwide, there has been little functional investigation of early tumor dissemination in this disease.

However, circulating epithelial cells have been detected in the blood of some patients that are prone to colorectal cancer such as those with intestinal polyps[8] and inflammatory bowel diseases including Crohn's syndrome[9]. Moreover, In 2019, a computational study on metastatic samples from patients with colorectal cancer proposed that the metastatic seeding occurs early, when the tumor is not clinically detectable and years before diagnosis and surgery[10]. Therefore, reaching a comprehensive understanding of the mechanisms underlying early colorectal cancer (CRC) spread is essential for developing effective therapeutic strategies to delay or prevent metastasis.

To this end, we have generated an inducible transgenic mouse model that enables us to track early dissemination of intestinal tumorigenesis. This mouse model expresses tdTomato in the whole intestinal epithelium and spontaneously develops intestinal adenomas due to *Apc* mutation, which mimics the early stages of the disease.

Using this mouse, we provide the first evidence of the early dissemination of intestinal cells and suggest that, in synergy with systemic factors (TIMP1, TNF-α, SDF-1, CXCL2, and M-CSF), these cells induce liver remodeling that increases the permissiveness of this organ for later metastasis-initiating cells.

These findings shed light on the complex molecular and cellular mechanisms involved in metastasis, which begins earlier than previously believed, and highlight a potential role of early-disseminated tumor cells in driving this process.

RESULTS

Validation of the transgenic mouse model and detection of early intestinal cells in the liver

To promote early lesions in the intestine and track potential early dissemination, we generated an inducible transgenic mouse model, named AVCT, with three elements: *Apc*, which is considered as the gatekeeper for intestinal tumorigenesis and is mutated in the vast majority of intestinal tumors[11], *Villin*-CreERT2 where the CreERT2 recombinase is under the control of the intestine-specific *Villin* promoter and tdTomato. In this model, upon tamoxifen treatment, the recombinase translocates into the nucleus and thus becomes active, specifically in the epithelial compartment of the intestine. This drives both the expression of tdTomato in every recombined epithelial cell of the intestine and, simultaneously, the deletion of exon 14 in only one allele of the *Apc* gene. Intestinal tdTomato-positive adenoma will then form from rare cells that underwent a second hit of the WT *Apc* allele (Figure 1A).

Heterozygosity of *APC* is key for this study to slow down the process of intestinal tumorigenesis and recapitulate human pathology. Importantly, control mice for all the experiments, named VCT, have no Apc mutation but still express tdTomato in all intestinal epithelial cells upon tamoxifen treatment.

All the results presented here were obtained 4–5 months after tamoxifen treatment, which is considered as an early stage of intestinal tumorigenesis. At this age, intestinal adenomas were identified by a pathologist as high-grade dysplasia, with no observed concurrent carcinoma lesions. In addition, metastases were never observed at distant organs.

The first validation step of this model revealed that tdTomato is indeed expressed throughout the intestine in AVCT mice and in wild type *Apc* control VCT mice. Equally importantly, after 4-5 months there were newly formed adenomas in the AVCT mice but, as predicted, not in the VCT control (Figure 1B). In addition, Figure 1C shows diffuse **β**-catenin localization in intestinal adenomas, indicating that the Wnt signaling pathway is activated, as expected for *Apc* mutant tumors[12].

Having established our cell-traceable intestinal adenoma model, we wanted to know whether intestinal tdTomato-positive cells could disseminate and be found in distant organs at the adenoma stages. Since the liver is the main organ of metastasis in colorectal cancer, we have focused on this organ. Strikingly we observed single cells as well as clusters of a few cells expressing tdTomato by immunohistochemistry (Figure 1D). In addition, livers were cleared and stained to visualize early-disseminated intestinal cells in the whole liver. In Figure 1E, the upper-left panel clearly shows intestinal tdTomato-positive cells sited in the liver of AVCT mice.

Figure 1E upper-right and lower panels, show stack areas from different liver regions that present single or clusters of these disseminated tdTomato-positive cells (in white).

To determine whether the early dissemination we had observed was likely a global patho physiological response to intestinal tumorigenesis, we used an alternative mouse model by exposing VCT mice to AOM, a carcinogen agent, and DSS, a pro-inflammatory factor (Supplementary Figure S1A)[13].

Similarly, in our experimental, pathologist has confirmed that the intestine only bears adenomas (Supplementary Figure S1B), validating that this model also allowed the focus on very early stages of intestinal tumorigenesis. In the liver of these mice, 3 months post-treatment, tdTomato-positive intestinal cells could also be detected by immunohistochemistry at an early stage of tumor development (Supplementary Figure S1C).

Early dissemination correlates with myeloid cell enrichment in the liver

AVCT mice never develop liver metastases over the course of their lives. In addition, once intestinal adenoma cells are injected either subcutaneously or orthotopically in the caecum of highly immunodeficient mice, these cells never grow into tumors (data not shown), strongly suggesting that adenoma cells are not tumorigenic. We thus wanted to assess the impact of early dissemination in the liver. To address this question, we profiled at the single-cell level the mRNA expression of dissociated liver cells from AVCT and VCT mice 5 months post-tamoxifen administration. In the AVCT mouse, the UMAP representation shows a significant change in the liver landscape, particularly an important increase in the myeloid cell population including macrophages, neutrophils and dendritic cells (DCs) (Figures 2A-C). Differential expression analysis of AVCT versus VCT myeloid cells and the subsequent gene set enrichment analysis (GSEA) revealed prominent enrichment in Gene Ontology (GO) terms related to immune responses, such as activation and migration of myeloid leukocytes, regulation of the inflammatory response, and regulation of TNF superfamily cytokine production (Figure 2D and Data S1). Interestingly, high enrichment scores were also detected for non-immune related terms like ‘cell junction organization and the presence of ‘collagen-containing extracellular matrix’, suggesting that myeloid cells could induce a matrix remodeling. To further investigate specific features related to macrophage and neutrophil enrichment in AVCT mouse liver, we subset all the annotated myeloid cells and re-analyzed them (Figure 2E). There was a clear accumulation of dendritic cells, recruited macrophages, and neutrophils in AVCT, which was highly specific, as Kupffer cells remained similar in VCT and AVCT mice (Figure 2F).

This re-clustering allowed the distinction of 12 sub-clusters with unique gene expression patterns, including three different groups of both neutrophils (clusters N1, N4, and N6) and

macrophages (clusters M3, M5, and M7), which facilitated the identification of those molecular phenotypes more associated with AVCT (Figure 2G-I).

Overall, the liver of VCT mouse had one main cluster of neutrophils (Cluster N1) and a few cells of another cluster (Cluster N6), whereas the AVCT mouse liver presented the three detected clusters N1, N4, and N6, indicating an enrichment and a greater functional diversity among neutrophil subpopulations in mice bearing intestinal adenomas. Similarly, a common cluster of macrophages is present in both mouse genotypes (Cluster M7), whereas two additional differentiated subpopulations were almost exclusive to AVCT (Clusters M3 and M5). For neutrophils, the top markers of AVCT-specific clusters N4 and N6 exhibit a gene expression profile similar to that of myeloid-derived suppressor cell-type neutrophils including expression of *Cebpe*, *Ltf*, *Cd177*, and *Ngp*[14] as presented in the heat map Figure 2 H.

In the highly enriched macrophage cluster of AVCT liver, Cluster M3 exhibits significant enrichment of genes involved in cell proliferation, including *Pclaf*, *Stmn1*, and *Mki67* (Supplementary Figure S2A). In contrast, Cluster M5 is characterized by enrichment of genes associated with cell migration, such as *Ahnak*, *Ccr2*, and fibronectin-1 (*Fn1*), and enrichment of GO terms associated with extracellular matrix (ECM) (Supplementary Figure S2B, C). Interestingly, Fn1 has been described for its role in macrophage polarization towards an immunosuppressive phenotype (M2)[15]. Particularly, this cluster also displays increased expression of inflammatory chemokines, including *Ccl9* and to a lesser extent *Ccl3*, that are described for their role in recruiting myeloid progenitors into the pre-metastatic niche[16]. In addition, CCR2, the receptor of CCL2 is also overexpressed in the M5 cluster. Importantly, the CCL2-CCR2 signaling axis has been shown to induce the recruitment of other immune cells to create an immunosuppressive environment. The VCT and AVCT common M7 cluster exhibits expression of genes involved in antigen presentation and phagocytic functions, including CD74, H2-Eb1, H2-Aa, and Axl, thereby suggesting a putative physiological role for this cluster (Supplementary Figure S2D).

The striking myeloid-derived suppressor cell-like signature found in N4 and N6 neutrophil clusters specifically in the liver of AVCT mice at adenoma stage of tumor development, along with the increased abundance of macrophages with an inflammatory profile in the AVCT mouse liver, prompted us to validate this myeloid cell enrichment at the protein level.

Liver remodeling is early induced during intestinal tumorigenesis

We thus employed a multiplexing immunolabelling technology (CyTOF/Hyperion technology) to validate the myeloid cell enrichment in the liver of AVCT mice. A panel of 12 antibodies was used to assess the hepatic microenvironmental changes at early stages. Figure 3A shows a representative region, stained with this panel, where myeloid cells are visualized (including

myeloid cells that are labeled with CD11b, macrophages with CD68, neutrophils with MPO, dendritic cells with cd11c), along with lymphocytes that were labelled with CD3 and vessel wall and activated stellate cells with α-sma1. According to cell quantification on 3 different regions of interest from 3 different mice, only macrophages and neutrophils were significantly enriched (Figure 3B). We therefore focused our attention to these cell types. Immunohistochemistry using Iba1 (Figure 3C) and MPO (Figure 3D) antibodies validates macrophage and neutrophil enrichment on a larger group of mice (n≥6). Quantification of signal intensities demonstrates that the myeloid enrichment in the liver of AVCT mice is statistically significant compared to the liver of VCT mice. In addition, by using CD68 and F4-80 antibodies to stain macrophages, we show similar results, as presented in Supplementary Figures S3A and S3B, respectively.

We then first performed staining using iba1 and CD68 antibodies for macrophages as well as MPO for neutrophils on liver sections from the complementary AOM/DSS-treated mice (supplementary Figure S3C). Similar results were observed in this model.

To exclude any potential bias effect of the AVCT model (including tamoxifen and exon 14 deletion of one of the *Apc* allele), we also validated myeloid cell enrichment in the liver of *ApcΔ*14 and *Apc*^{1638N} mice, two distinct mouse models that spontaneously develop intestinal adenomas[17,18] (Supplementary Figure S3D). Importantly, all these mouse models have an aberrant activation of the Wnt signaling pathway due to either an APC mutation (for AVCT, *ApcΔ*14 and *Apc*^{1638N}) or to β-catenin mutation (for the majority of AOM/DSS cases[19]). Similarly, we observed a slight macrophage enrichment in the liver of mice for which intestinal tumorigenesis has been induced by a BRAFV600E mutation[20], suggesting that myeloid cell enrichment induced by early dissemination could be a global feature of early intestinal tumorigenesis independent of the initial driver mutation (Supplementary Figure S3E).

Then, because early dissemination has been well described in other cancers, we obtained liver sections of PanIN stages from KPC (KrasG12D/+; Trp53 Pdx1-Cre) mice and BRAFV600E/cdkn2a young mice for pancreatic cancer and melanoma, respectively. In these livers, we confirmed macrophage and neutrophil enrichment using Iba1 and MPO antibodies, respectively, demonstrating that early dissemination correlates with myeloid cell enrichment in several distinct solid tumors (Supplementary Figure S4 A-D).

Early-intestinal disseminated cells in synergy with circulating cytokines recruit myeloid cell in the liver

We showed a clear correlation between the presence of early-disseminated tumor cells and hepatic enrichment of myeloid cells. Importantly, examination of the distribution of the myeloid cells revealed that myeloid cells enrichment was observed throughout the tissue (Figure 3). We therefore sought to investigate the impact of the presence of these intestinal disseminated

cells on the transcriptional program of the neighborhood liver cells. GeoMx digital spatial profiler technology was employed to determine hepatic gene expression in different regions in the vicinity (presence of tdTomato-positive intestinal cells) or in greater distance (absence of tdTomato-positive intestinal cells) in AVCT mice, which were compared to areas from VCT mice as a control (Figure 4A). The Volcano plot in Figure 4B demonstrates that the transcriptional program is modified in the neighborhood of early-disseminated intestinal cells in the liver of AVCT mice. Furthermore, gene ontology analysis of the upregulated genes in the adjacent areas of early intestinal disseminated cells in AVCT revealed the activation of TNFα signaling via NF-kB. This signaling pathway is a commonly activated pathway when inflammation is occurring (Figure 4C)[21]. This suggests that early-disseminated intestinal cells have a local impact on the liver.

Since NF-kB is a transcription factor highly involved in the regulation of cytokine expression, we compared the plasma of AVCT and VCT mice using a cytokine array. Four cytokines out of a total of 42 were overrepresented in the plasma of AVCT mice (CXCL2, M-CSF, SDF-1, and TIMP-1). Using ELISA, we quantified the plasma levels of these candidates in addition to TNF-α and found that they were significantly elevated in AVCT mice relative to VCT mice (Figure 4D). In fact, SDF-1, known to induce hepatic myeloid cell infiltration when systemically elevated, belongs to the adenoma-induced set of cytokines. Interestingly, TIMP-1 is the most-upregulated systemic factor, which prepares a liver-specific pre-metastatic niche that is composed of broad infiltration of myeloid cells[23].

We next wondered whether early-disseminated intestinal cells, alone in the liver, could directly induce myeloid cell enrichment. To test this, we injected a small number (1000) of intestinal adenoma cells in the spleens of WT mice to let these cells rapidly reach the liver[22] (Figure 4E). We could observe a significant macrophage and neutrophil enrichment compared to PBS-injected mice (Figure 4F), demonstrating that early-disseminated intestinal cells alone cause myeloid cell enrichment even in the absence of a primary tumor.

Notably, the same pattern of systemic factors, CXCL2, SDF-1, TIMP-1, and TNF-α were also overrepresented in the plasma of WT mice injected with small number of adenoma cells in their livers (Figure 4G). This suggests that the increased circulating factor level in the plasma of AVCT mice is not only due to adenoma secretion but is also a direct consequence of the presence of early-disseminated tumor cells in the liver. As a proof of concept that injected adenoma-induced TIMP-1 is sufficient to induce myeloid-recruiting SDF-1 we repeated the experiment detailed in Figure 4E but in addition, TIMP1 was intraperitonially administered. Interestingly, a synergistic effect was observed in mice that have received both intestinal adenoma cell injection and exogenous TIMP1 (Figure 4H). Figure 4I shows similar results as expected because a feed-forward loop exists between TIMP1 and SDF-1 secretion as previously described in the literature[23].

Altogether, these results demonstrate that early intestinal disseminated cells in the liver and systemic factors act in synergy at adenoma stage to remodel the liver and prepare a pre-metastatic niche early during tumorigenesis.

To highlight the clinical significance of selected cytokines, we measured TNF-α, CXCL-2, M-CSF, SDF-1, and TIMP-1 levels in the blood of ten patients with intestinal adenomas and ten healthy individuals, using ELISA. These cytokine candidates were more abundant in the blood of patients with intestinal adenomas, confirming results obtained in mice (Figure 4J).

Early liver remodeling enhances metastatic cell colonization.

Next, we investigated the functional impact of early liver remodeling, concomitant with early dissemination, on its metastatic colonization. We recapitulated this process by injecting syngeneic carcinoma cells (MC38) in the spleen of VCT or AVCT mice (Figure 5A). MC38 cells are known to be able to colonize the liver after their injection in the spleen of immunocompetent mice[24]. However, here our intention was to challenge metastasis initiation ability. Therefore, we injected a moderate number of cells (100,000 cells) and sacrificed the first mice after only 15 days. In these conditions, we detected visible micro-metastases only in the remodeled liver of AVCT mice (data not shown).

When, in the same experiment, mice were sacrificed after 30 days, as expected, metastases were also detected in the liver of VCT mice. However, there were less metastases in this control group as compared to the AVCT group. Indeed, more than half of the VCT mice had no detectable metastasis, whereas AVCT mice presented statistically more liver metastases (chi-square test; p value = 0.014, Figure 5B). In addition, metastases in the remodeled liver of AVCT mice were significantly larger than those that developed in the normal liver of VCT mice (Figure 5C-E).

It is noteworthy that similar results were observed in two additional mouse models (*Apc*^{Min} and *Apc*^{lox15}) when the murine carcinoma CMT93 cell line injection was used to induce metastasis, and the metastatic colonization was assessed by luciferase assay (Supplementary figure S. 5 A, B and C, D respectively)

Altogether, these results demonstrate that early-disseminated intestinal cells in synergy with systemic factors induce liver remodeling, which subsequently enhances colonization and metastasis in the liver.

DISCUSSION

In this work, we used various complementary mouse models to demonstrate that intestinal tumors spread at an adenoma stage during tumorigenesis. Moreover, we confirmed that the early spread of intestinal cells, along with the secretion of some factors, is associated with an enrichment of neutrophils and macrophages in the liver, as well as matrix remodeling. Finally, we demonstrated that the liver remodeling that occurs at an early stage promotes the later colonization of this organ and metastatic development.

It was previously believed that tumor dissemination only occurred during the later, malignant, stages of tumor development. However, some disseminated tumor cells detected in patients with melanoma, pancreatic, and breast cancer harbored a lower mutation burden than primary tumors, suggesting that dissemination may occur during the early stages of tumor evolution[2,25,26]. In breast cancer for example, consecutive papers have decoded cell signaling associated with early dissemination by proving that a sub-population of $Her2^{+}p\text{-}p38^{lo}p\text{-}Atf2^{lo}Twist1^{hi}E\text{-}cad^{lo}$ cancer cells spread early to target organs by activating a Wnt-dependent epithelial-mesenchymal transition (EMT)-like dissemination program[27,28].

At late stages of tumor development, the premetastatic niche has been well described in the literature by several groups[29–31]. They have shown that the pre-metastatic niche can be prepared through a complex interplay between circulating factors secreted by primary advanced tumors, the immune system, and local stromal components. Indeed, many cytokines, such as TIMP-1 or SDF-1[23], are first released by tumor cells and then secreted by myeloid and stromal cells, creating a vicious circle that prepares the soil for disseminated cells to seed and colonize distant organs. Other components such as exosomes, miRNA, cell-free circulating DNA, and lncRNA have also been proposed to be part of this process[32,33].

However, our novel findings presented here reveal that the preparation of pre-metastatic niches takes place at adenoma stage of intestinal tumorigenesis. Moreover, we demonstrate that early-disseminated cells, in synergy with systemic factors, exert an impact on the hepatic microenvironment, promoting metastasis development.

In recent years, tumor dormancy has emerged as a promising process to target. Indeed, disseminated tumor cells can infiltrate, enter into cell cycle arrest in distant organs and can remain dormant for varying amounts of time. The present work diverges from this theory because early-disseminated tumor cells have a significant impact on hepatic subpopulations, which strongly suggests that they secrete factors and respond to extracellular signals and thus are probably not dormant. Nevertheless, the fact that AVCT mice do not develop liver metastases, even after one year, strongly suggests that the early-disseminated tumor cells observed in the liver of 4–5-month-old animals are not cycling.

To further decipher the mechanisms involved in early dissemination, aging will be an important parameter to consider. In the present work, it is important to note that the microenvironment in young mice used in our study may not fully reflect the human aged pathology. In fact, recent research has shown that fibroblasts in aging mice may play a critical role in regulating tumor cell proliferation inducing a phenotype switching from a dormant to a proliferative state through Wnt5a secretion[34].

Early dissemination includes primary tumor cell departure to reach distant organs as well as circulating factors secreted by either adenomas or recruited immune and stromal cells.

In this work, we have focused our analysis on systemic factors that are differentially represented in the plasma of AVCT mice in comparison with VCT mice. This comparative analysis was performed first with a cytokine array, and the top candidates were quantified by ELISA. Four cytokines were selected; namely TIMP1, M-CSF, SDF-1, and CXCL2, as well as TNF- α, that are all associated with macrophage and neutrophil recruitment in cancer of various organs[22,36–42] and could, thus, explain the myeloid cell enrichment observed in the liver of AVCT mice.

For example, TIMP-1 has been found to correlate with poor prognosis in several cancers, including colorectal cancer, where it has been associated with liver metastasis and tumor relapses upon comparing its plasmatic level in patients with different stages of CRC. In the same study, authors nicely showed that TIMP-1 helps prepare the premetastatic niche, notably through neutrophil recruitment thanks to the SDF-1/CXCR4 axis. However, they did not quantify the level of TIMP-1 in the plasma of either healthy donors or patients with intestinal adenomas, whereas we show that this increase is very early during intestinal tumorigenesis both in mice and humans. CXCL2 is primarily produced by neutrophils and binds to CXCR2, which in turn couples with Gαi to stimulate neutrophils and thus initiate a vicious circle [42,43]. Then, CCL2 produced by tumor cells, is an important chemokine for the recruitment and retention of macrophages, which could partially explain macrophage enrichment in the liver of AVCT mice. Finally, TNF-α activates NF-kB, a well-known transcription factor regulating the expression of many cytokines, including TIMP1, M-CSF, SDF-1, and CXCL2 [21,35,36,44].

Interestingly, the immunosuppressive phenotype highlighted by single-cell RNA sequencing has been nicely illustrated through intravital live imaging. Indeed, in mouse liver exhibiting early dissemination, metastatic cells were completely ignored by neutrophils and macrophages (supplementary video S1), in contrast to control mice where myeloid cells attacked metastatic cells (supplementary video S2 and S3).

In conclusion, our present work advances the understanding of tumor dissemination in the context of intestinal tumorigenesis. Using different elegant mouse models, we have

demonstrated that this process starts at adenoma stage. Furthermore, our findings suggest that early disseminated cells, in synergy with systemic factors, trigger significant changes in the liver microenvironment. These changes create a permissive microenvironment, forming the early pre-metastatic niche and promoting the colonization of metastatic cells. Our study has significant implications not only for fundamental cancer research but also for clinical practice, as we have identified systemic factors (TNF-α, TIMP1, M-CSF, SDF-1, and CXCL2) that are overrepresented in the blood of patients with benign intestinal adenomas, and could be used as potential biomarkers.

Acknowledgements

Authors would like to acknowledge cytometry and mass imaging (CIM), Montpellier Rio Imaging (MRI) and iexplore facilities. Authors would like to thank Julian Venables (Science sense) for the manuscript editing. Finally, authors are grateful to Pr E. Charafe-Jauffret for her precious pathologist expertise on mouse intestinal lesions.

Funding

This research was publicly funded through the I-SITE Excellence Program of the University of Montpellier, part of the Investments France 2030; Institut national du cancer (INCA, PLBIO22-084) and SIRIC: Grant “INCa-DGOS-Inserm 6045”. ZH has been funded by “fondation pour la recherche médicale” and ZH and GB have been funded by “la ligue contre le cancer”.
AK was supported by grants from the Deutsche Forschungsgemeinschaft (DFG) (KR2047/ 8-1 and KR2047/15-1).

Author contributions

Conceptualization, Z.H, G.B, P.J., and J.P. Methodology, Z.H, G.B, E.S, F.G., C.P., A.E., A.T., Z.W., C.B., and J.P.; Investigation, Z.H, G.B, T.L., J.S., C.B., L.B., C.P, M.N., C.B., P.G., and A.T. Formal Analysis; L.B., Z.H, G.B, Z.W., C.B., and J.P Writing – Original Draft, Z.H, and J.P.; Writing – Review & Editing, G.B., P.J., D.G., F.L., C.B., and A.K.; Funding Acquisition, Z.H., F.L., and J.P.; Resources, J.G.G, M.L., L.L.C., S.F., R.R., D.H, A.K., J.F.B., and O.S.; Supervision, J.P.

Declaration of interests

Authors declare no conflict of interest

Figure legends:

Figure 1: **Generation and validation of the transgenic mouse model and early detection of intestinal cells in the liver**

(A) Schematic representation of the VCT and AVCT mouse models employed in the study. Tamoxifen administration in these models induces tdTomato expression in intestinal epithelial cells. In AVCT mice, tamoxifen additionally induces a mutation in one APC allele. This gatekeeper of intestinal tumorigenesis is then subject to a second hit in rare cells that will initiate adenoma formation.

(B) Immunohistochemistry on intestinal swiss roll sections demonstrates a high recombination efficiency of tamoxifen treatment in the AVCT mouse and control VCT mice. The resulting expression of tdTomato all intestinal epithelial cells is revealed by RFP antibody staining. Adenomas are visible in the AVCT mice (zoom in). Black crosses indicate intestinal adenomas.

(C) Immunofluorescence on an adenoma of AVCT mouse adenoma, using anti RFP (red) and anti β-catenin (green) antibodies, shows that adenomas express tdTomato and have abnormally high Wnt signaling pathway activity, illustrated by cytoplasmic/nuclear diffused β-catenin accumulation compared to adjacent normal tissue.

(D) Immunohistochemistry using RFP antibody on liver sections from 6 different AVCT mice, sacrificed between 2-5 months post tamoxifen, reveals the presence of rare tdTomato positive early-disseminated tumor cells (black arrows).

(E) Tissue clearing of the liver using vDisco and its imaging using Miltenyi Ultramicroscope Blaze. Reconstitution of a whole 3D liver lobe stained with NanoTag FluoTag-Q anti-RFP (in red) and Propidium Iodide (in turquoise) to label cell nuclei (Upper panel, left). Raw images of different areas of the livers presenting early-disseminated tumor cells (red arrows, NanoTag FluoTag-Q anti-RFP in white) (upper panel, right and lower panel)

Figure 2: **Early dissemination correlates with myeloid cell enrichment in the liver of AVCT mice**

(A) Uniform manifold approximation and projection (UMAP) integrated analysis of AVCT and VCT liver cells labeled according to their classification by ScType

(B) UMAP cells labeled according to their classification by ScType and splitted by condition AVCT vs VCT

(C) The subpopulation composition of each animal.

(D) Selected Gene Ontology gene-sets enriched in AVCT myeloid cell populations compared with VCT. NES, normalized enrichment score

(E) UMAP plot displaying the integrated re-analysis of myeloid cell populations, colored according to Seurat re-clustering.

(F, G) UMAP splitting AVCT/VCT of myeloid cells, labelled according to Sctype annotation (G), and highlighting the specific neutrophil and macrophages subclusters.

(H, I) Heatmap of the top 15 differentially expressed markers defining each neutrophil (H) and macrophage (I) subpopulation.

Figure 3: **Liver remodeling is early induced during intestinal tumorigenesis**

(A) Representative Cytof/hyperion image of liver sections from VCT mice (left) and AVCT mice (right) after induction reveals a strong dysregulation in different immune populations; macrophages are labeled with CD68 in yellow and cd11b in white; neutrophils are labelled with MPO in red; dendritic cells with CD11c in magenta and vessel walls and activated stellate cells with a-sma1 in green.

(B) Number of cells expressing macrophage marker (CD68); myeloid cells (CD11b). Neutrophil marker (MPO) and dendritic cells (CD11c) per region of interest (ROI). Columns, mean; Bars. SD; Students t test. *, $P<0.05$; **, $P<0.01$

(C) Immunohistochemistry using Iba1 antibody to detect macrophages on liver sections from VCT mice (left panel) and AVCT intestinal adenoma bearing mice (middle panel). Right panel shows signal intensity quantification. Violin plot Students t test n>14 **** p value <0.0001

(D) Immunohistochemistry using MPO antibody to detect macrophages on liver sections from VCT mice (left panel) and AVCT intestinal adenoma bearing mice (middle panel). Right panel shows signal intensity quantification. Violin plot Students t test n>6, **** p value <0.0001

Figure 4: **Early-intestinal disseminated cells in synergy with circulating cytokines recruit myeloid cell in the liver**

(A) Examples of chosen regions of interest, for spatial transcriptomic analysis, on liver sections, from VCT and AVCT mice, containing or not intestinal early-disseminated tumor cells expressing tdTomato.

(B) Volcano plot depicting transcriptional differences highlighted by spatial transcriptomic analysis on liver sections from AVCT mice containing or not intestinal early-disseminated tumor cells.

(C) Heatmap showing TNF-α signaling activation on regions of interest containing intestinal early-disseminated tumor cells expressing tdTomato on AVCT mouse liver sections.

(D) Cytokine (TIMP1, SDF-1, M-CSF, TNF-α and CXCL2) level fold change, in the plasma of AVCT mice, compared to VCT mice, assessed by ELISA. Columns, mean; Bars. SD; Students t test. ***; $P<.001$; ****, $P<.0001$

(E) Schematic description of adenoma cells injected in the spleen of WT mice to assess the impact, of early-disseminated tumor cells alone, on myeloid cell enrichment in the liver. IS: Intrasplenic injection

(F) Immunohistochemistry using F4-80 antibody (top panel) to detect macrophages and MPO antibody (bottom panel) on liver sections from WT mice injected with PBS or adenoma cells in their spleen. Right panel shows signal intensity quantification of each marker. Columns, mean; Bars. SD; Students t test F4-80: n=5 * p value= 0.0307; MPO n=3 * p value= 0.0334

(G) Cytokine (TIMP1, SDF-1, M-CSF, TNF-α and CXCL2) level fold change, assessed by ELISA, in the plasma of WT mice, injected with adenoma cells into their spleen, compared to WT mice injected with PBS Columns, mean; Bars. SD; Students t test. **, *P*<0.01 ***; *P*<0.001; ****, *P*<0.0001

(H) Timp1 plasmatic level assessed by ELISA in PBS intrasplenically injected mice with PBS followed by PBS treatment (IS PBS+ PBS); in PBS intrasplenically injected mice with PBS followed by Timp1 treatment (IS PBS+ Timp1); in intrasplenically injected mice with adenoma cells followed by PBS treatment (IS adenoma cells+ PBS) and in intrasplenically injected mice with adenoma cells followed by Timp1 treatment (IS adenoma cells+ Timp1). Columns, mean; Bars. SD; Students t test. ***; *P*<0.001; ****, *P*<0.0001.

(I) SDF-1 plasmatic level assessed by ELISA in PBS intrasplenically injected mice with PBS followed by PBS treatment (IS PBS+ PBS); in PBS intrasplenically injected mice with PBS followed by Timp1 treatment (IS PBS+ Timp1); in intrasplenically injected mice with adenoma cells followed by PBS treatment (IS adenoma cells+ PBS) and in intrasplenically injected mice with adenoma cells followed by Timp1 treatment (IS adenoma cells+ Timp1) Columns, mean; Bars. SD; Students t test. ***; *P*<0.001; ****, *P*<0.0001.

(J) Cytokine (TIMP1, SDF-1, M-CSF, TNF-α and CXCL2) level fold change, in the plasma of patients bearing intestinal adenomas, compared to the plasma of healthy donors, assessed by ELISA. Columns, mean; Bars. SD; Students t test. *, *P*<0.05; **, *P*<0.01, ***; *P*<0.001; ****, *P*<0.0001.

Figure 5: Early liver remodeling enhances metastatic cell colonization

(A) Schematic description of 100 000 MC38 carcinoma cells injected in the spleen of VCT or AVCT (13 and 10 mice respectively) to assess the impact of liver remodeling on the success of late metastatic cell colonization.

(B) Number of VCT and AVCT mice developing no tumor, or less or more than 10 liver metastases following MC38 cell injection in the spleen.

(C) Mean of liver metastasis, with a size lower than 10 $mm^{2,}$ in VCT and AVCT mice 30 days after MC38 cell injection in the spleen. Columns, mean; Bars. SEM; Students t test. *; *P*<0.05

(D) Representative photos of liver with metastases from VCT and AVCT mice 30 days following MC38 cell injection in the spleen

(E) Representative hematoxylin and eosin staining of liver sections with metastases from VCT and AVCT mice 30 days following MC38 cell injection in the spleen

STAR Methods

Transgenic mouse models

All mice were housed in a SPF environment. All animal experiments were approved by the French Agriculture and Forestry Ministry (APAFIS number 20720- 2019051314421302).

Generating the AVCT mouse model

To create the *Apc*, Villin, Cre, Tomato mouse used in this paper we used *Apc*$^{lox/lox}$ and *Villin*^{CreERT2} transgenic (AV) that have been previously described[17]. These *Apc*$^{lox/lox}$; *Villin*^{CreERT2} bigenic mice were crossed with Ai14 reporter mice [45](JAX:007908) where a lox-P flanked stop cassette prevents the expression of the red fluorescent protein, tdTomato. 6-8 weeks old transgenic descendent mice *Apc* $^{lox/WT}$; *Villin*^{CreERT2}; Ai14$^{KI/WT}$ were put on a tamoxifen diet (0.5g/kg tamoxifen+5% saccharose) SAFE®E8220 for 2 weeks to induce recombination in all intestinal epithelial cells. The percentage of tdTomato-positive intestinal crypts was analyzed using immunohistochemistry on whole intestinal swiss rolls (n=4), reporting recombination of ~90%. Female and male mice were used in all the experiments, and they were all of mixed genetic backgrounds (C57BL/6J and 129S6). Livers from these mice were harvested 4-5 months post-tamoxifen administration.

Other mouse models employed in this study

Apc$^{Min/+}$ mice (Jackson Laboratories) and Apc15$^{Lox/+}$;villinCre were maintained on C57BL/6 background. *Apc*$^{15Lox/+}$;*Villin*Cre were established by breeding Apc15$^{Lox/Lox}$ (provided by Dr. Riccardo Fodde, Netherland) with *Villin*Cre (provided by Dr. Averil Ma, USCF). ACTB-ECFP mice and c-fms-EGFP transgenic mouse lines were maintained in-house and crossed with Apc$^{Min/+}$ to get Apc$^{Min/+}$ /ACTB-ECFP/cfms-EGFP mice for intravital imaging. All mouse experiments were approved by the Institutional Animal Care and Use Committee of University of California, San Francisco.

The *Apc*$^{\Delta 14}$ mouse model was previously described[17]. Mice were sacrificed at the age of 3 months for further investigations.

Livers from *Apc* ^{1638N} mutant mice (previously described in[18,46]) were kindly provided by S. Fre lab .

FFPE liver sections from BRAFV600E *Villin*Cre were kindly provided by Owen Sansom. The mouse model was previously described[20].

FFPE liver sections from KPC mice, sacrificed at PANIN stage, were kindly given by Dr Guillermet-Guibert in CRCT in Toulouse; the mouse model was previously described[47].
FFPE liver sections from a melanoma mouse model were kindly given by Dr. Le Cam in IRCM in Montpellier. Briefly in the mouse model (Braf^{tm1Cpri}; Cdkn2a^{tm1Rdp}; Rosa26^{Tomato}; Tg(Tyr-cre/ERT2), melanomas appears in an average between 6 and 9 months after TAM application on animals harboring the Cdkn2a_null allele at the homorozygote stage. Liver sections were obtained from animals sacrificed 7 months post TAM where no signs of liver metastases were observed.

Chemically induced colorectal cancer

The AOM/DSS colon carcinogenesis model is largely described [48]. Villin^{CreERT2}/Ai14$^{KI/WT}$ mice were first put on a tamoxifen diet (0.5g/kg tamoxifen+5% saccharose) SAFE®E8220 for 2

weeks, to induce the tdTomato expression in all intestinal epithelial cells. 2-3-month-old mice received a single intraperitoneal injection of Azoxymethane (AOM) (10mg/kg body weight, 250 ng/mouse) (Sigma #A5486) followed by dextran sodium sulfate (DSS) administration (2% in drinking water) 1 week after the AOM injection for five consecutive days. 2 additional cycles of DSS were administered with a 1-week break (Fig. Supp. 1). Mice were monitored daily for body weight change and health status. Mice were sacrificed 2-3 months after the end of the protocol.

Adenoma culture

$APC^{lox/WT}$ /$Villin^{CreERT2}$ /$Ai14^{KI/WT}$ mice aged 4 months were sacrificed, and intestinal adenomas were micro-dissected using forceps and micro-dissection scissors. Adenomas were dissociated using a mouse tumor dissociation kit (Miltenyi) following manufacturer's protocol. Dissociated adenoma cells were passed through a 70µm cell strainer, centrifuged, suspended in DMEM-F12 (Gibco), and plated in 50% Matrigel drops in 12-well plates. After Matrigel polymerization, the drop was covered with DMEM-F12 medium supplemented with EGF, N2, and glutamine. This culture medium ensured the expansion of transformed cells only.

Cell Culture.

Murine colon cancer cell line (MC38) was purchased from ATCC. CMT93 mouse rectum cancer cell line (provided by Dr. Fabrice Pierre, Unité Mixte de Recherche 1089, Toulouse, France) express an mCherry fluorescent tag and luciferase reporter (CMT93-mCh-Luc). These cell lines were cultured in DMEM (Gibco) containing 10% FCS and 1% penicillin/streptomycin at 37°C under 5% CO2.

Sample preparation

Livers from *Apc*$^{lox/WT}$/*Villin*^{CreERT2}/$Ai14^{KI/WT}$ and *Villin*^{CreERT2}/$Ai14^{KI/WT}$ mice were harvested at 5 months post-tamoxifen administration. Dissected livers were digested using a cocktail of Collagenase I (100mg/g of liver weight), Hyaluronidase (100mg/g), and DNAse (1.25 mg/g) in RPMI medium at 37°C under agitation for 45 minutes. Digested cells were passed through a 70µm cell strainer and centrifuged to remove the enzymatic solution. Red blood cells were removed using red blood lysis buffer (Miltenyi) and dead cells were removed using a debris removal kit (Miltenyi) according to manufacturer's protocol. Live cells were sorted using sytox green dye on a FACSariaII (BD). Sorted cells were directly processed into the scRNA sequencing experiment.

Single-cell RNA sequencing

Demultiplexing, quality control and analysis

Image analyses and base calling were performed using the NovaSeq Control Software and the Real-Time Analysis component (Illumina). Demultiplexing was performed using the 10X Genomics software Cellranger mkfastq (v6.1.1), a wrapper of Illumina's software bcl2fastq (v2.20)]. The quality of the raw data was assessed using FastQC (v0.11.9) from the Babraham Institute and the Illumina software SAV (Sequencing Analysis Viewer). FastqScreen (v0.15.0) was used to estimate the potential level of contamination.
Cell suspensions were loaded on a Chromium controller (10x Genomics, Pleasanton, CA, USA) to generate single-cell Gel Beads-in-Emulsion (GEMs). Single-cell RNAseq libraries

were prepared using a Chromium Single cell 3'RNA Gel Bead and Library Kit V3.1 (P/N 10000268, 1000120, PN-1000215 10x Genomics). GEM-RT was performed in a C1000 Touch Thermal cycler with 96-Deep Well Reaction Module (Bio-Rad; P/N 1851197): 53°C for 45 min, 85°C for 5 min; held at 4°C. After RT, GEMs were broken and the single-strand cDNA was cleaned up with DynaBeads MyOne Silane Beads (Thermo Fisher Scientific; P/N 37002D). cDNA was amplified using the C1000 Touch Thermal cycler with 96-DeepWell Reaction Module: 98°C for 3 min; 12 cycles of 98°C for 15 s, 63°C for 20 s, and 72°C for 1 min; 72°C for 1 min; held at 4°C. The amplified cDNA product was cleaned up with SPRIselect beads (SPRI P/N B23318). Dual Indexed sequencing libraries were constructed with SPRIselect following these steps: (1) Fragmentation end repair and A-tailing and size selection; (2) adapter ligation and cleanup; (3) sample index PCR and size selection. The barcode sequencing libraries were quantified by quantitative PCR (KAPA Biosystems Library Quantification Kit for Illumina platforms P/N KK4824). Sequencing libraries were loaded at 200 pM on an Illumina NovaSeq6000 using the following read length: 28 bp Read1, 10 bp I7 Index, 10 bp I5 Index, 90 bp Read2.

Data analysis:

Alignment, gene expression quantification, and statistical analysis were performed using the Cell Ranger Single Cell Software Suite from 10× Genomics, Inc., against their pre-built Mus Musculus's GRCm39 reference genome. To discard ambient RNA falsely identified as cells, the Cell Ranger count was run a second time with the option –force-cells to force the number of cells to detect. 'Cell Ranger aggr' was then used to combine each sample result into one single analysis. Data processing and visualization were performed with Seurat package v4.3.0[49,50]. A total of 2,446 cells with >30,000 counts and from 500 to 6,000 expressed genes were considered for VCT, whereas 2,569 cells with >55,000 counts and from 500 to 7,000 genes were considered for AVCT. Raw unique molecular identifier counts were log-normalized and the top 2,000 highly variable genes were identified using the *FindVariableFeatures* function. To account for biological and technical batch differences between animals, the Seurat anchor-based integration workflow was followed[51]. After integration, gene expression was scaled and principal component analysis was performed using the *RunPCA* function considering 20 principal components. Next, the *RunUMAP*, *FindNeighbors* and *FindClusters* functions were applied, based on the first 10 principal components, with a cluster resolution set to 0.5. The number of components was determined based on the elbow plot. Cell type assignment was automatically performed using ScType[52] with a customized version of the cell marker database (Data S2). Briefly, we selected and manually curated the top-scored differentially expressed genes identified per cell type in the total mouse liver cell atlas provided by Guilliams M et al. Table S1[49], excepting the Hepatic Stem and Progenitor Cells (HSPCs).

Analysis of Myeloid Cells

The *FindMarkers* function using Wilcoxon rank sum test was then used to identify differentially expressed genes between VCT and AVCT for all the annotated myeloid cell populations (i.e., dendritic cells, recruited Macrophages, Kupffer Cells and Neutrophils) from raw counts, using thresholds of genes detected in >20% of cells, showing >0.25 $\log_2$-transformed fold-change and adjusted p-value <0.05. Gene Set Enrichment Analysis was performed using the dedicated function from ClusterProfileR[53], ranking genes by the $\log_2$-transformed average fold-change and using Gene Ontology gene sets obtained from the msigdbr package (v7.5.1)[54]. The significance cutoff was set at 5% Benjamini-Hochberg (BH) FDR.

Non-myeloid cells were then removed, and the dataset was normalized, integrated and analyzed again following the same procedure described above. In this case, the *FindAllMarkers* function was used to identify differentially expressed genes between all the re-defined clusters of myeloid cells, considering 'only positives' markers and thresholds of genes detected in >15% of cells and showing >0.15 log_2-transformed fold change. Due to the reduced number of cells and to obtain a more confident approximation of the functional diversity of these subclusters, gene set enrichment analysis only included markers with an adjusted p-value <0.01. Additionally, incorporated the REACTOME gene set, and the significance cutoff of the enriched pathways was set at 1% (BH) FDR for neutrophils and 0.1% for macrophages.

Spatial transcriptomic analysis:

The Technology Access Program (TAP) from Nanostring Technology in Seattle, USA, was used to run GeoMx digital spatial profiler on liver FFPE sections. Briefly, 3 FFPE liver sections from different AVCT mice and 2 FFPE sections from different VCT mice were stained with morphological markers: PanCK, iba1, TdTomato (for early-disseminated tumor cells) and DAPI along with oligo-conjugated antibodies. Custom regions of interest were assigned either 'close to' or 'far from' early-disseminated tumor cells, and randomly selected regions were picked from VCT sections. From these regions, barcodes were cleaved using UV light in the GeoMX digital spatial profiler instrument, then hybridized, and finally counted using the Ncounter system. A remote access to the data, allowed the analysis of the data along with quality control assessment, normalization, and differential expression gene evaluation between the different regions of interest. Differential gene expression was evaluated by Linear Mixed Model (LMM) test with BH correction. Volcano plot was constructed using VolcaNoseR web page[55].

Immunolabelling

Tissues were fixed using 10% buffered formalin overnight at room temperature and embedded into paraffin using Spin Tissue Processor STP 120. 4 µm sections of FFPE tissue were used for immunolabeling. Sections were first dewaxed by heating them to 56°C, immersed in five serial xylene baths, and then dehydrated in serial ethanol baths. Antigens were unmasked using either boiling citrate pH 6.2 or boiling tris-base pH 9 for 20 minutes. Non-specific sites and permeabilization were done using a blocking buffer (TBS containing 5% Donkey serum, 0.2% Triton X-100) for at least 30 minutes. Sections were then incubated with primary antibodies (diluted in blocking buffer) overnight at 4°C. The next day, slides were washed and then incubated with the secondary antibody at room temperature for 1 hour.

For immunofluorescence staining, fluorescent secondary antibodies (donkey Fluor 488 anti mouse; donkey 547 Fluor anti-rabbit (from Jackson Immuno Research) were used, and nuclei were stained with DAPI. Slides were mounted using fluoromount G and were observed using an epifluorescent microscope (Zeiss AxioImager Z1)

For immunohistochemistry staining, the endogenous peroxidase activity was quenched using hydrogen peroxide/methanol 1.5% for 20 minutes at room temperature before applying the primary antibody. The secondary antibodies we used are coupled to peroxidase (Histofine). Staining development was done using FastDAB followed by hematoxylin counterstaining. Slides were then mounted using Pertex and then scanned with a NanoZoomer 2.0 HT (Hamamatsu)

CyTOF/Hyperion assay

Antibodies and Metal Conjugation

Antibodies were conjugated using the Maxpar® X8 Antibody Labeling Kit according to the manufacturer's instructions (PRD002 Rev 14, Fluidigm, Standard Biotools).

Imaging mass cytometry

4µm FFPE tissue sections were deparaffinized and rehydrated and subsequently submitted to heat-induced epitope/antigen retrieval for 30 minutes at 96 °C using the Dako Target Retrieval Solution at pH 9 (S236784-2, Agilent technologies) in water.
Unspecific antibody staining was blocked with Superblock™ (37515, ThermofisherScientific) at room temperature (RT) for 45 min, and then with FcR Blocking Reagent (130-092-575, Miltenyi) at RT for 1h. Slides were washed in PBS/0.2% Triton X-100 (PBS-T) and incubated with a metal-tagged antibody cocktail at 4°C overnight. After washes in PBS-T, nuclei were stained with iridium (1:400 in PBS; Fluidigm, Standard Biotools) for 30min at RT, washed in PBS and then in distilled water for 5min and dried at RT for 30 min.
Pre-selected regions of interest were acquired with the Hyperion Imaging System (Fluidigm, Standard Biotools) by a UV laser ablation at 200Hz. Data were exported as MCD files and visualized using the Fluidigm MCD™ viewer 1.0.560.6.
Cell segmentation was obtained using the ImcSegmentationPipeline[56]. Briefly, MCD files were first converted to TIFF format. Then pixel classification was done with Ilastik v1.3.3[57] and applied to images with CellProfiler v4.1.3[58] software to generate the segmentation mask and the corresponding single-cell file (.fcs) using the R package flowCore version 2.6.0.

Intrasplenic injection

Amplified culture adenoma cells (as previously described above) were dissociated using gentle cell dissociation reagent and labeled with green dead cell stain for cell sorting. Green negative cells were sorted in a BD FACSAria II. 1000 cells were resuspended in 50 µl of PBS and injected into the spleen of C57BL6J female mice aged 6-8 weeks.

Murine colon cancer cell line (MC38) was used to establish a model of liver metastasis. Intrasplenic injection was done as previously described[22]. Briefly, 100,000 live cells were resuspended in 50ul of PBS and injected into the spleen of VCT and AVCT mice 5 months post-tamoxifen administration. 5 minutes after the injection, spleens were removed and mice were then sacrificed 1 month after the injection.

Timp1 administration

Timp1 recombinant protein was generously provided by Achim Kruger. Mice were treated every second day by intraperitoneal injection of 4,93 ug recombinant Timp1 protein per injection.

Splenic Injection for in vivo liver metastasis experiments (IVIS)

Mice were anesthetized with isoflurane (Henry Schein) and small incisions were made on the skin and peritoneum of left lateral flank to exteriorize spleen. $2x10^6$ CMT93-mCh-Luc cells in

50 µl Dulbecco's PBS (D-PBS) were then injected into spleen, followed by closure of incisions with sutures and surgical staples. Mice were monitored after surgery. Bioluminescence imaging was performed using an IVIS Spectrum and image radiance values were normalized using Living Image (Caliper LifeScience). Living Image Software (PerkinElmer, Waltham, MA, USA) was used to analyze the signals in manually selected regions of interest. Data were expressed as photons per second per square centimeter per steradian (p/s/cm^2/sr).

ELISA

For mouse plasma, samples were diluted to one-third. ELISA for Timp-1 and SDF-1 (from R&D systems); M-CSF, CXCL2 and TNF- α (from Preprotech 900-M54) was performed according to manufacturer's protocol

For human plasma, samples were diluted to one-third and ELISA for Timp-1(Preprotech 900-M438), M-CSF (R&D systems DMC00B), CXCL2 (Preprotech 900-M120), SDF-1 Preprotech 900-M92) and TNF- α (DTA00D) was performed according to manufacturer's protocol**.**

Tissue clearing

Perfusion-fixed mice were processed for active whole-body vDISCO labelling as described previously[59]. Briefly after decolorization, decalcification and permeabilization, mice were perfused for 6d with 250ml of the same permeabilization solution containing 35 µl of nanobooster, (NanoTag FluoTag-Q) 1:7,000 in dilution and 290µl of Propidium Iodide (PI, to label cell nuclei). Mice were then incubated for an additional 2 days with the same labeling solution refreshed with an extra 5µl of nanobooster. Finally, the mice were cleared according to the vDISCO protocol. The cleared livers of the animals were imaged using Miltenyi Ultramicroscope Blaze with a 4x objective.

Intravital Imaging

The intravital spinning-disk confocal microscopy, surgical procedures, and anesthesia of mice were done as described previously[60]. Briefly, a microlensed spinning-disk confocal scan head (CSU-10b, Yokogawa Corporation; modified by Solamere Technology Group) was coupled to a motorized, inverted fluorescence microscope (Zeiss Axiovert 200M inverted fluorescence microscope; Carl Zeiss) and four-color imaging achieved using an argon laser for 488-nm excitation, a krypton laser for 568 and 647 excitation or solid-state 561-nm and 640-nm lasers, a 405-nm solid-state laser, and selective emission filters. Images were collected with an intensified charge-coupled device camera (XR-Mega-10EX S-30; Stanford Photonics). Live, long-term, multi-position imaging using a robotic stage was performed with 10×Fluar 0.5 NA or 20× Fluar 0.75 NA lens air objectives, using the Micro-Manager software. Mice were initially anesthetized with 4% isoflurane (at 21% oxygen, balance nitrogen; Summit Anesthesia Solutions), and surgery was performed with 2.5% (vol/vol) isoflurane. Before surgery, mice received retro-orbitally 7 µg of Alexa Fluor 647-conjugated Ly-6G antibody. The ventral surface of the mouse was prepared for surgery with isopropyl alcohol or betadine, a ventral midline incision made with sterilized scissors, the liver was surgically exposed and a glass microscope slide glued below the left lobe of the liver. Then, 2x10^6 CMT93-mCh-Luc cells in 50 µl Dulbecco's PBS (D-PBS) were injected into the spleen. The glass slide was rotated to expose the inner surface of the liver, and the mouse was transferred to the microscopic stage. During imaging, isoflurane was reduced to the lowest concentration at which the mouse did not react to pain, typically 0.8–1.0%. We used an oximeter probe (MouseOx, Starr Life Sciences) to monitor and display the heart rate, the arterial oxygen saturation of the blood, and the

distension of blood vessels caused by the pulse and the breathing, adjusting the anesthesia levels appropriately to the individual mouse. During the imaging procedure, isoflurane was delivered in a humidified mix of nitrogen and oxygen [at least 21% (vol/vol)], with oxygen adjusted to achieve >95% oxygen saturation of arterial blood as measured with an oximeter probe. Mice were covered with a recirculating heated water blanket during imaging (Gaymar). Time-lapse videos were assembled using Bitplane Imaris (v6.3–7.6 for Windows 64×), adjusting brightness and contrast for clarity, as well as applying smoothing filters to reduce noise.

Patient samples:

Blood from patients with intestinal adenomas was obtained within the clinical trial NCT05648240 and patients all gave their consent.

Supplementary Video S1-3

Videos from intravital live imaging on the liver of $Apc^{Min/+}$ /ACTB-ECFP/cfms-EGFP mouse (S1) and APC WT/ACTB-ECFP/cfms-EGFP mice (S2-3) 15 minutes post intrasplenic injection of CMT93 expressing mcherry. Macrophages are visualized in green, CMT93 tumor cells in red, hepatocytes in blue and neutrophils in white. For further details refer to method section.

References

1. Mehlen, P., and Puisieux, A. (2006). Metastasis: a question of life or death. Nat. Rev. Cancer *6*, 449–458. 10.1038/nrc1886.

2. Rhim, A.D., Mirek, E.T., Aiello, N.M., Maitra, A., Bailey, J.M., McAllister, F., Reichert, M., Beatty, G.L., Rustgi, A.K., Vonderheide, R.H., et al. (2012). EMT and dissemination precede pancreatic tumor formation. Cell *148*, 349–361. 10.1016/j.cell.2011.11.025.

3. Schwartz, R.S., and Erban, J.K. (2017). Timing of Metastasis in Breast Cancer. N. Engl. J. Med. *376*, 2486–2488. 10.1056/NEJMcibr1701388.

4. Werner-Klein, M., Scheitler, S., Hoffmann, M., Hodak, I., Dietz, K., Lehnert, P., Naimer, V., Polzer, B., Treitschke, S., Werno, C., et al. (2018). Genetic alterations driving metastatic colony formation are acquired outside of the primary tumour in melanoma. Nat. Commun. *9*, 1–17. 10.1038/s41467-017-02674-y.

5. Dudgeon, C., Harris, C.R., Chen, Y., Ghaddar, B., Sharma, A., Shah, M.M., Roberts, A.I., Casabianca, A., Collisson, E.A., Balachandran, V.P., et al. (2020). A Novel Model of Pancreatic Cancer Dormancy Reveals Mechanistic Insights and a Dormancy Gene Signature with Human Relevance. bioRxiv, 2020.04.13.037374. 10.1101/2020.04.13.037374.

6. Rahrmann, E.P., Shorthouse, D., Jassim, A., Hu, L.P., Ortiz, M., Mahler-Araujo, B., Vogel, P., Paez-Ribes, M., Fatemi, A., Hannon, G.J., et al. (2022). The NALCN channel regulates metastasis and nonmalignant cell dissemination. Nat. Genet. *54*, 1827–1838. 10.1038/s41588-022-01182-0.

7. Liu, R. Dormancy of disseminated prostate cancer cells in the bone cortex is induced by osteoblasts. https://www.biorxiv.org/content/10.1101/2022.09.02.506436v2.

8. Tsai, W.-S., Chen, J.-S., Shao, H.-J., Wu, J.-C., Lai, J.-M., Lu, S.-H., Hung, T.-F., Chiu, Y.-C., You, J.-F., Hsieh, P.-S., et al. (2016). Circulating Tumor Cell Count Correlates with Colorectal Neoplasm Progression and Is a Prognostic Marker for Distant Metastasis in Non-Metastatic Patients. Sci. Rep. *6*, 24517. 10.1038/srep24517.

9. Pantel, K., Denève, E., Nocca, D., Coffy, A., Vendrell, J.-P., Maudelonde, T., Riethdorf, S., and Alix-Panabières, C. (2012). Circulating epithelial cells in patients with benign colon diseases. Clin. Chem. *58*, 936–940. 10.1373/clinchem.2011.175570.

10. Hu, Z., Ding, J., Ma, Z., Sun, R., Seoane, J.A., Scott Shaffer, J., Suarez, C.J., Berghoff, A.S., Cremolini, C., Falcone, A., et al. (2019). Quantitative evidence for early metastatic seeding in colorectal cancer. Nat. Genet. *51*, 1113–1122. 10.1038/s41588-019-0423-x.

11. Kinzler, K.W., and Vogelstein, B. (1996). Lessons from hereditary colorectal cancer. Cell *87*, 159–170. 10.1016/s0092-8674(00)81333-1.

12. Morin, P.J., Sparks, A.B., Korinek, V., Barker, N., Clevers, H., Vogelstein, B., and Kinzler, K.W. (1997). Activation of beta-catenin-Tcf signaling in colon cancer by mutations in beta-catenin or APC. Science *275*, 1787–1790. 10.1126/science.275.5307.1787.

13. Parang, B., Barrett, C.W., and Williams, C.S. (2016). AOM/DSS Model of Colitis-Associated Cancer. Methods Mol. Biol. Clifton NJ *1422*, 297–307. 10.1007/978-1-4939-3603-8_26.

14. Veglia, F., Hashimoto, A., Dweep, H., Sanseviero, E., De Leo, A., Tcyganov, E., Kossenkov, A., Mulligan, C., Nam, B., Masters, G., et al. (2021). Analysis of classical neutrophils and polymorphonuclear myeloid-derived suppressor cells in cancer patients and tumor-bearing mice. J. Exp. Med. *218*. 10.1084/jem.20201803.

15. Wang, H., Zhang, J., Li, H., Yu, H., Chen, S., Liu, S., Zhang, C., and He, Y. (2022). FN1 is a prognostic biomarker and correlated with immune infiltrates in gastric cancers. Front. Oncol. *12*, 918719. 10.3389/fonc.2022.918719.

16. Yan, H.H., Jiang, J., Pang, Y., Achyut, B., Lizardo, M., Liang, X., Hunter, K., Khanna, C., Hollander, C., and Yang, L. (2015). CCL9 induced by TGF-β signaling in myeloid cells enhances tumor cell survival in the premetastatic organ. Cancer Res. *75*, 5283–5298. 10.1158/0008-5472.CAN-15-2282-T.

17. Colnot, S., Niwa-Kawakita, M., Hamard, G., Godard, C., Le Plenier, S., Houbron, C., Romagnolo, B., Berrebi, D., Giovannini, M., and Perret, C. (2004). Colorectal cancers in a new mouse model of familial adenomatous polyposis: influence of genetic and environmental modifiers. Lab. Investig. J. Tech. Methods Pathol. *84*, 1619–1630. 10.1038/labinvest.3700180.

18. Smits, R., van der Houven van Oordt, W., Luz, A., Zurcher, C., Jagmohan-Changur, S., Breukel, C., Khan, P.M., and Fodde, R. (1998). Apc1638N: a mouse model for familial adenomatous polyposis-associated desmoid tumors and cutaneous cysts. Gastroenterology *114*, 275–283. 10.1016/s0016-5085(98)70478-0.

19. Zeineldin, M., and Neufeld, K.L. (2015). New insights from animal models of colon cancer: inflammation control as a new facet on the tumor suppressor APC gem. Gastrointest. Cancer Targets Ther. *5*, 39–52. 10.2147/GICTT.S51386.

20. Rad, R., Cadiñanos, J., Rad, L., Varela, I., Strong, A., Kriegl, L., Constantino-Casas, F., Eser, S., Hieber, M., Seidler, B., et al. (2013). A Genetic Progression Model of BrafV600E-Induced Intestinal Tumorigenesis Reveals Targets for Therapeutic Intervention. Cancer Cell *24*, 15–29. 10.1016/j.ccr.2013.05.014.

21. Taniguchi, K., and Karin, M. (2018). NF-κB, inflammation, immunity and cancer: coming of age. Nat. Rev. Immunol. *18*, 309–324. 10.1038/nri.2017.142.

22. Belthier, G., Homayed, Z., Bouclier, C., Asari, M., and Pannequin, J. (2021). Circulating Tumor Cell Lines: an Innovative Tool for Fundamental and Translational Research. J. Vis. Exp. JoVE. 10.3791/62329.

23. Seubert, B., Grünwald, B., Kobuch, J., Cui, H., Schelter, F., Schaten, S., Siveke, J.T., Lim, N.H., Nagase, H., Simonavicius, N., et al. (2015). Tissue inhibitor of metalloproteinases (TIMP)-1 creates a premetastatic niche in the liver through SDF-1/CXCR4-dependent neutrophil recruitment in mice. Hepatol. Baltim. Md *61*, 238–248. 10.1002/hep.27378.

24. Dupaul-Chicoine, J., Arabzadeh, A., Dagenais, M., Douglas, T., Champagne, C., Morizot, A., Rodrigue-Gervais, I.G., Breton, V., Colpitts, S.L., Beauchemin, N., et al. (2015). The Nlrp3 Inflammasome Suppresses Colorectal Cancer Metastatic Growth in the Liver by Promoting Natural Killer Cell Tumoricidal Activity. Immunity *43*, 751–763. 10.1016/j.immuni.2015.08.013.

25. Schmidt-Kittler, O., Ragg, T., Daskalakis, A., Granzow, M., Ahr, A., Blankenstein, T.J.F., Kaufmann, M., Diebold, J., Arnholdt, H., Muller, P., et al. (2003). From latent

disseminated cells to overt metastasis: genetic analysis of systemic breast cancer progression. Proc. Natl. Acad. Sci. U. S. A. *100*, 7737–7742. 10.1073/pnas.1331931100.

26. Eyles, J., Puaux, A.-L., Wang, X., Toh, B., Prakash, C., Hong, M., Tan, T.G., Zheng, L., Ong, L.C., Jin, Y., et al. (2010). Tumor cells disseminate early, but immunosurveillance limits metastatic outgrowth, in a mouse model of melanoma. J. Clin. Invest. *120*, 2030–2039. 10.1172/JCI42002.

27. Harper, K.L., Sosa, M.S., Entenberg, D., Hosseini, H., Cheung, J.F., Nobre, R., Avivar-Valderas, A., Nagi, C., Girnius, N., Davis, R.J., et al. (2016). Mechanism of early dissemination and metastasis in Her2+ mammary cancer. Nature *540*, 588–592. 10.1038/nature20609.

28. Hosseini, H., Obradović, M.M.S., Hoffmann, M., Harper, K.L., Sosa, M.S., Werner-Klein, M., Nanduri, L.K., Werno, C., Ehrl, C., Maneck, M., et al. (2016). Early dissemination seeds metastasis in breast cancer. Nature *540*, 552–558. 10.1038/nature20785.

29. Doglioni, G., Parik, S., and Fendt, S.-M. (2019). Interactions in the (Pre)metastatic Niche Support Metastasis Formation. Front. Oncol. *9*. 10.3389/fonc.2019.00219.

30. Pein, M., Insua-Rodríguez, J., Hongu, T., Riedel, A., Meier, J., Wiedmann, L., Decker, K., Essers, M.A.G., Sinn, H.-P., Spaich, S., et al. (2020). Metastasis-initiating cells induce and exploit a fibroblast niche to fuel malignant colonization of the lungs. Nat. Commun. *11*, 1–18. 10.1038/s41467-020-15188-x.

31. Liu, Y., and Cao, X. (2016). Characteristics and Significance of the Pre-metastatic Niche. Cancer Cell *30*, 668–681. 10.1016/j.ccell.2016.09.011.

32. Costa-Silva, B., Aiello, N.M., Ocean, A.J., Singh, S., Zhang, H., Thakur, B.K., Becker, A., Hoshino, A., Mark, M.T., Molina, H., et al. (2015). Pancreatic cancer exosomes initiate pre-metastatic niche formation in the liver. Nat. Cell Biol. *17*, 816–826. 10.1038/ncb3169.

33. Liu, Y., and Cao, X. (2016). Characteristics and Significance of the Pre-metastatic Niche. Cancer Cell *30*, 668–681. 10.1016/j.ccell.2016.09.011.

34. Fane, M.E., Chhabra, Y., Alicea, G.M., Maranto, D.A., Douglass, S.M., Webster, M.R., Rebecca, V.W., Marino, G.E., Almeida, F., Ecker, B.L., et al. (2022). Stromal changes in the aged lung induce an emergence from melanoma dormancy. Nature *606*, 396–405. 10.1038/s41586-022-04774-2.

35. Bommarito, A., Richiusa, P., Carissimi, E., Pizzolanti, G., Rodolico, V., Zito, G., Criscimanna, A., Di Blasi, F., Pitrone, M., Zerilli, M., et al. (2011). BRAFV600E mutation, TIMP-1 upregulation, and NF-κB activation: closing the loop on the papillary thyroid cancer trilogy. Endocr. Relat. Cancer *18*, 669–685. 10.1530/ERC-11-0076.

36. Penzo, M., Habiel, D.M., Ramadass, M., Kew, R.R., and Marcu, K.B. (2014). Cell migration to CXCL12 requires simultaneous IKKα and IKKβ-dependent NF-κB signaling. Biochim. Biophys. Acta *1843*, 1796–1804. 10.1016/j.bbamcr.2014.04.011.

37. Zhang, H., Ye, Y.-L., Li, M.-X., Ye, S.-B., Huang, W.-R., Cai, T.-T., He, J., Peng, J.-Y., Duan, T.-H., Cui, J., et al. (2017). CXCL2/MIF-CXCR2 signaling promotes the recruitment of myeloid-derived suppressor cells and is correlated with prognosis in bladder cancer. Oncogene *36*, 2095–2104. 10.1038/onc.2016.367.

38. Seubert, B., Grünwald, B., Kobuch, J., Cui, H., Schelter, F., Schaten, S., Siveke, J.T., Lim, N.H., Nagase, H., Simonavicius, N., et al. (2015). Tissue inhibitor of

metalloproteinases (TIMP)-1 creates a premetastatic niche in the liver through SDF-1/CXCR4-dependent neutrophil recruitment in mice. Hepatol. Baltim. Md *61*, 238–248. 10.1002/hep.27378.

39. Lin, Y., Xu, J., and Lan, H. (2019). Tumor-associated macrophages in tumor metastasis: biological roles and clinical therapeutic applications. J. Hematol. Oncol.J Hematol Oncol *12*, 76. 10.1186/s13045-019-0760-3.

40. Gelmini, S., Mangoni, M., Serio, M., Romagnani, P., and Lazzeri, E. (2008). The critical role of SDF-1/CXCR4 axis in cancer and cancer stem cells metastasis. J. Endocrinol. Invest. *31*, 809–819. 10.1007/BF03349262.

41. Di Mitri, D., Mirenda, M., Vasilevska, J., Calcinotto, A., Delaleu, N., Revandkar, A., Gil, V., Boysen, G., Losa, M., Mosole, S., et al. (2019). Re-education of Tumor-Associated Macrophages by CXCR2 Blockade Drives Senescence and Tumor Inhibition in Advanced Prostate Cancer. Cell Rep. *28*, 2156-2168.e5. 10.1016/j.celrep.2019.07.068.

42. Chen, M.-C., Baskaran, R., Lee, N.-H., Hsu, H.-H., Ho, T.-J., Tu, C.-C., Lin, Y.-M., Viswanadha, V.P., Kuo, W.-W., and Huang, C.-Y. (2019). CXCL2/CXCR2 axis induces cancer stem cell characteristics in CPT-11-resistant LoVo colon cancer cells via Gαi-2 and Gαq/11. J. Cell. Physiol. *234*, 11822–11834. 10.1002/jcp.27891.

43. Girbl, T., Lenn, T., Perez, L., Rolas, L., Barkaway, A., Thiriot, A., del Fresno, C., Lynam, E., Hub, E., Thelen, M., et al. (2018). Distinct Compartmentalization of the Chemokines CXCL1 and CXCL2 and the Atypical Receptor ACKR1 Determine Discrete Stages of Neutrophil Diapedesis. Immunity *49*, 1062-1076.e6. 10.1016/j.immuni.2018.09.018.

44. Burke, S.J., Lu, D., Sparer, T.E., Masi, T., Goff, M.R., Karlstad, M.D., and Collier, J.J. (2014). NF-κB and STAT1 control CXCL1 and CXCL2 gene transcription. Am. J. Physiol. Endocrinol. Metab. *306*, E131-149. 10.1152/ajpendo.00347.2013.

45. Madisen, L., Zwingman, T.A., Sunkin, S.M., Oh, S.W., Zariwala, H.A., Gu, H., Ng, L.L., Palmiter, R.D., Hawrylycz, M.J., Jones, A.R., et al. (2010). A robust and high-throughput Cre reporting and characterization system for the whole mouse brain. Nat. Neurosci. *13*, 133–140. 10.1038/nn.2467.

46. Jacquemin, G., Wurmser, A., Huyghe, M., Sun, W., Homayed, Z., Merle, C., Perkins, M., Qasrawi, F., Richon, S., Dingli, F., et al. (2022). Paracrine signalling between intestinal epithelial and tumour cells induces a regenerative programme. eLife *11*. 10.7554/eLife.76541.

47. Thibault, B., Ramos-Delgado, F., Pons-Tostivint, E., Therville, N., Cintas, C., Arcucci, S., Cassant-Sourdy, S., Reyes-Castellanos, G., Tosolini, M., Villard, A.V., et al. (2021). Pancreatic cancer intrinsic PI3Kα activity accelerates metastasis and rewires macrophage component. EMBO Mol. Med. *13*. 10.15252/emmm.202013502.

48. Tanaka, T., Kohno, H., Suzuki, R., Yamada, Y., Sugie, S., and Mori, H. (2003). A novel inflammation-related mouse colon carcinogenesis model induced by azoxymethane and dextran sodium sulfate. Cancer Sci. *94*, 965–973. 10.1111/j.1349-7006.2003.tb01386.x.

49. Satija, R., Farrell, J.A., Gennert, D., Schier, A.F., and Regev, A. (2015). Spatial reconstruction of single-cell gene expression data. Nat. Biotechnol. *33*, 495–502. 10.1038/nbt.3192.

50. Hao, Y., Hao, S., Andersen-Nissen, E., Mauck, W.M., Zheng, S., Butler, A., Lee, M.J., Wilk, A.J., Darby, C., Zager, M., et al. (2021). Integrated analysis of multimodal single-cell data. Cell *184*, 3573-3587.e29. 10.1016/j.cell.2021.04.048.

51. Stuart, T., Butler, A., Hoffman, P., Hafemeister, C., Papalexi, E., Mauck, W.M., Hao, Y., Stoeckius, M., Smibert, P., and Satija, R. (2019). Comprehensive Integration of Single-Cell Data. Cell *177*, 1888-1902.e21. 10.1016/j.cell.2019.05.031.

52. Ianevski, A., Giri, A.K., and Aittokallio, T. (2022). Fully-automated and ultra-fast cell-type identification using specific marker combinations from single-cell transcriptomic data. Nat. Commun. *13*, 1–10. 10.1038/s41467-022-28803-w.

53. Yu, G., Wang, L.-G., Han, Y., and He, Q.-Y. (2012). clusterProfiler: an R package for comparing biological themes among gene clusters. Omics J. Integr. Biol. *16*, 284–287. 10.1089/omi.2011.0118.

54. Dolgalev I, I. (2022). MSigDB Gene Sets for Multiple Organisms in a Tidy Data Format. R package version 7.5.1.9001.

55. Goedhart, J., and Luijsterburg, M.S. (2020). VolcaNoseR is a web app for creating, exploring, labeling and sharing volcano plots. Sci. Rep. *10*, 1–5. 10.1038/s41598-020-76603-3.

56. Zanotelli, V. (2017). ImcSegmentationPipeline: A flexible multiplexed image segmentation pipeline based on pixel classification.

57. Berg, S., Kutra, D., Kroeger, T., Straehle, C.N., Kausler, B.X., Haubold, C., Schiegg, M., Ales, J., Beier, T., Rudy, M., et al. (2019). ilastik: interactive machine learning for (bio)image analysis. Nat. Methods *16*, 1226–1232. 10.1038/s41592-019-0582-9.

58. Stirling, D.R., Swain-Bowden, M.J., Lucas, A.M., Carpenter, A.E., Cimini, B.A., and Goodman, A. (2021). CellProfiler 4: improvements in speed, utility and usability. BMC Bioinformatics *22*, 433. 10.1186/s12859-021-04344-9.

59. Cai, R., Pan, C., Ghasemigharagoz, A., Todorov, M.I., Förstera, B., Zhao, S., Bhatia, H.S., Parra-Damas, A., Mrowka, L., Theodorou, D., et al. (2019). Panoptic imaging of transparent mice reveals whole-body neuronal projections and skull–meninges connections. Nat. Neurosci. *22*, 317–327. 10.1038/s41593-018-0301-3.

60. Lohela, M., Casbon, A.-J., Olow, A., Bonham, L., Branstetter, D., Weng, N., Smith, J., and Werb, Z. (2014). Intravital imaging reveals distinct responses of depleting dynamic tumor-associated macrophage and dendritic cell subpopulations. Proc. Natl. Acad. Sci. *111*, E5086–E5095. 10.1073/pnas.1419899111.

Figure 1

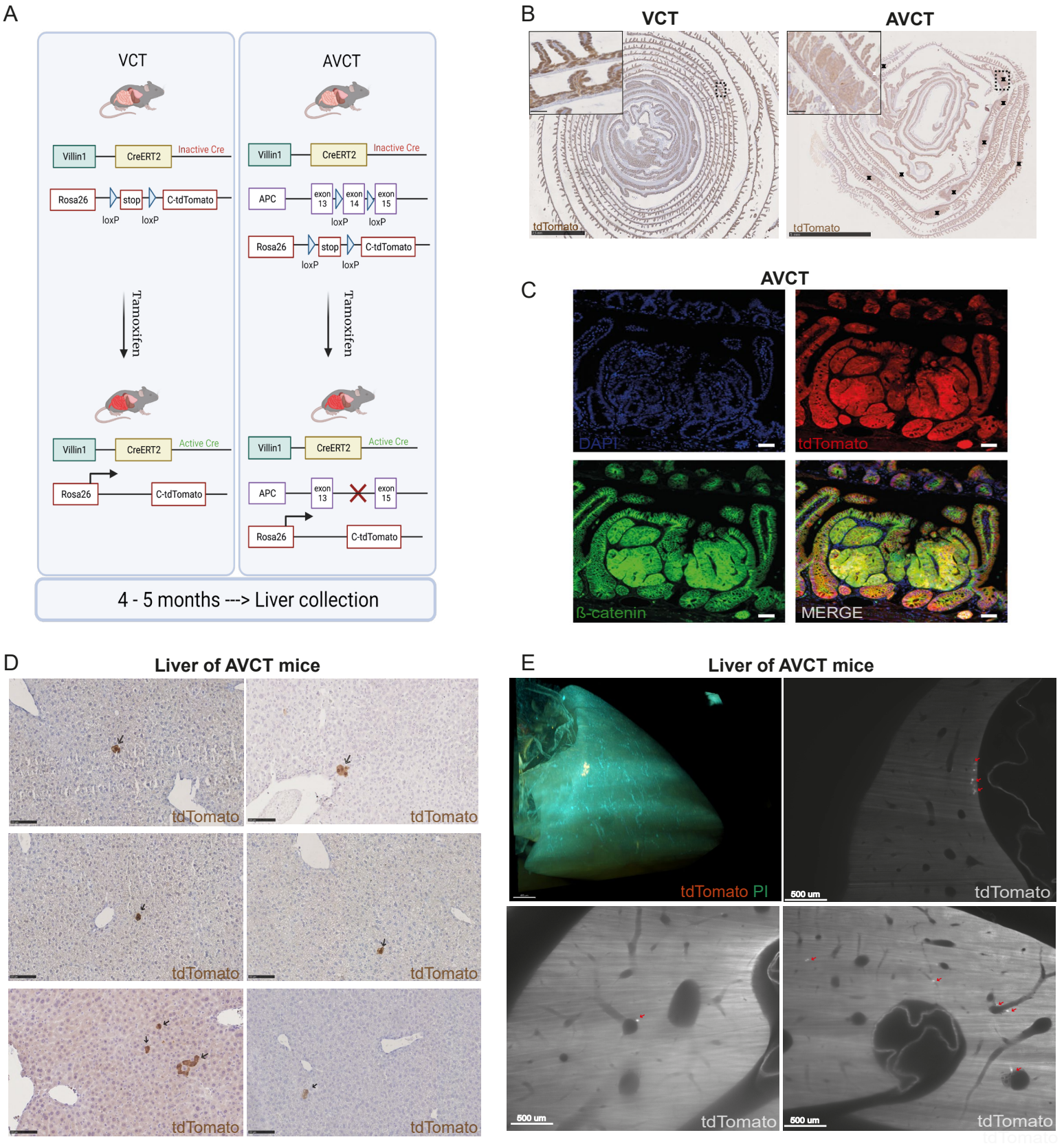

Figure 1

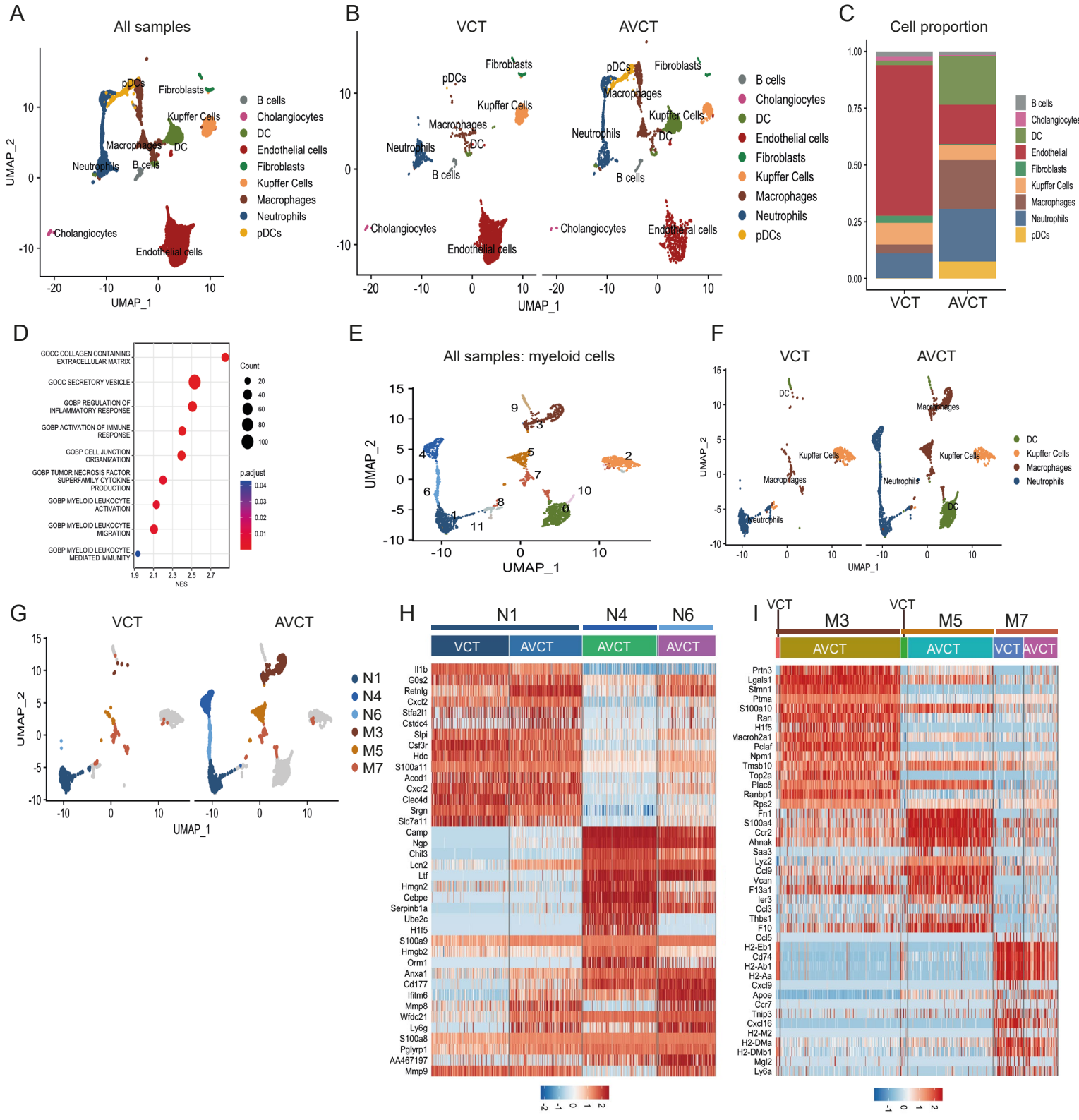
A
All samples
pDCs
Fibroblasts
Kupffer Cells
Macrophages
DC
Neutrophils
B cells
Cholangiocytes
Endothelial cells
UMAP_1
UMAP_2
B cells
Cholangiocytes
DC
Endothelial cells
Fibroblasts
Kupffer Cells
Macrophages
Neutrophils
pDCs
B
VCT
AVCT
C
Cell proportion
VCT
AVCT
D
GOCC COLLAGEN CONTAINING EXTRACELLULAR MATRIX
GOCC SECRETORY VESICLE
GOBP REGULATION OF INFLAMMATORY RESPONSE
GOBP ACTIVATION OF IMMUNE RESPONSE
GOBP CELL JUNCTION ORGANIZATION
GOBP TUMOR NECROSIS FACTOR SUPERFAMILY CYTOKINE PRODUCTION
GOBP MYELOID LEUKOCYTE ACTIVATION
GOBP MYELOID LEUKOCYTE MIGRATION
GOBP MYELOID LEUKOCYTE MEDIATED IMMUNITY
Count
p.adjust
NES
E
All samples: myeloid cells
F
G
N1
N4
N6
M3
M5
M7
H
I
Il1b
G0s2
Retnlg
Cxcl2
Stfa2l1
Cstdc4
Slpi
Csf3r
Hdc
S100a11
Acod1
Cxcr2
Clec4d
Srgn
Slc7a11
Camp
Ngp
Chil3
Lcn2
Ltf
Hmgn2
Cebpe
Serpinb1a
Ube2c
H1f5
S100a9
Hmgb2
Orm1
Anxa1
Cd177
Ifitm6
Mmp8
Wfdc21
Ly6g
S100a8
Pglyrp1
AA467197
Mmp9
Prtn3
Lgals1
Stmn1
Ptma
S100a10
Ran
H1f5
Macroh2a1
Pclaf
Npm1
Tmsb10
Top2a
Plac8
Ranbp1
Rps2
Fn1
S100a4
Ccr2
Ahnak
Saa3
Lyz2
Ccl9
Vcan
F13a1
Ier3
Ccl3
Thbs1
F10
Ccl5
H2-Eb1
Cd74
H2-Ab1
H2-Aa
Cxcl9
Apoe
Ccr7
Tnip3
Cxcl16
H2-M2
H2-DMa
H2-DMb1
Mgl2
Ly6a

Figure 3

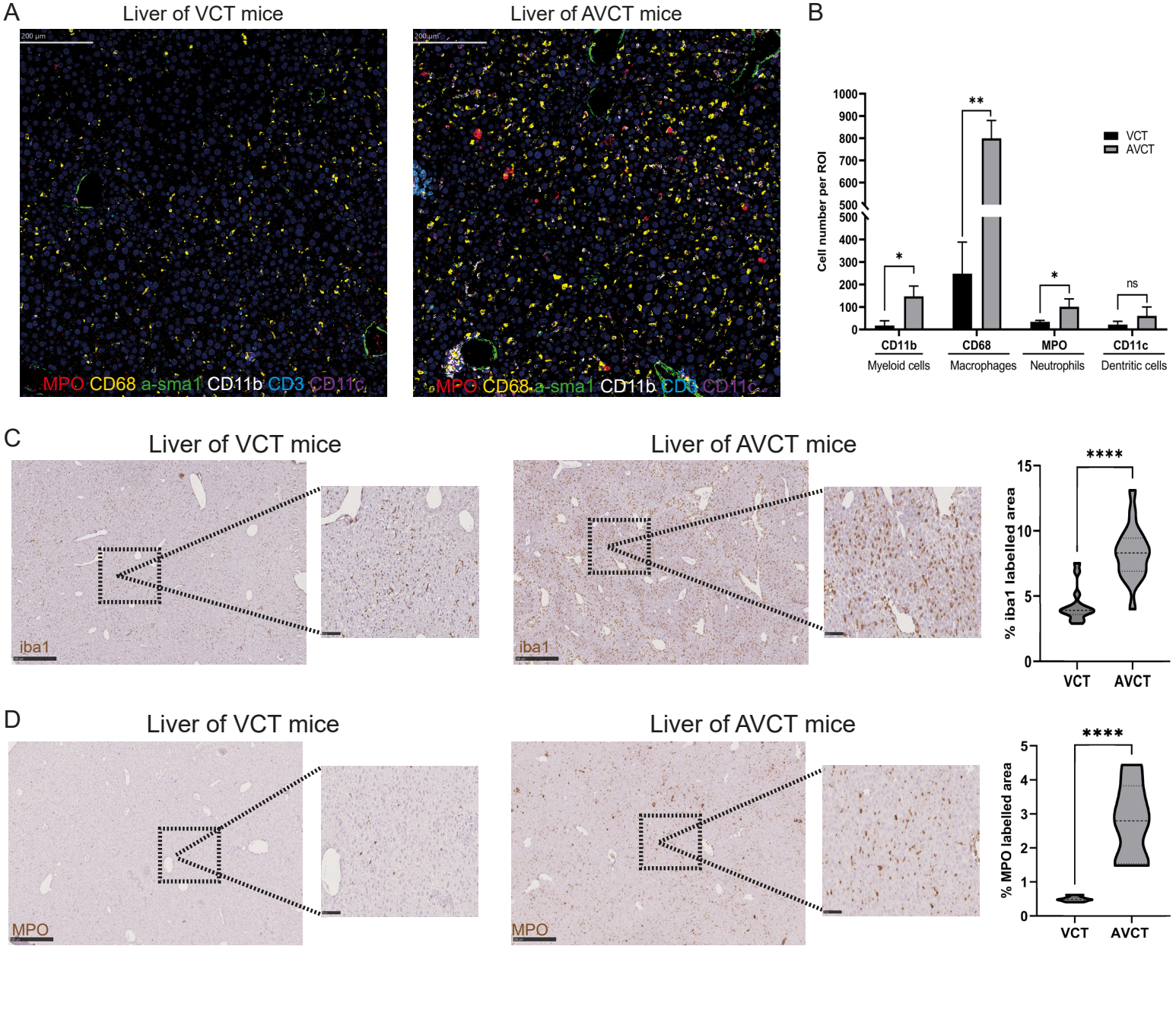

Figure 3

Figure 4

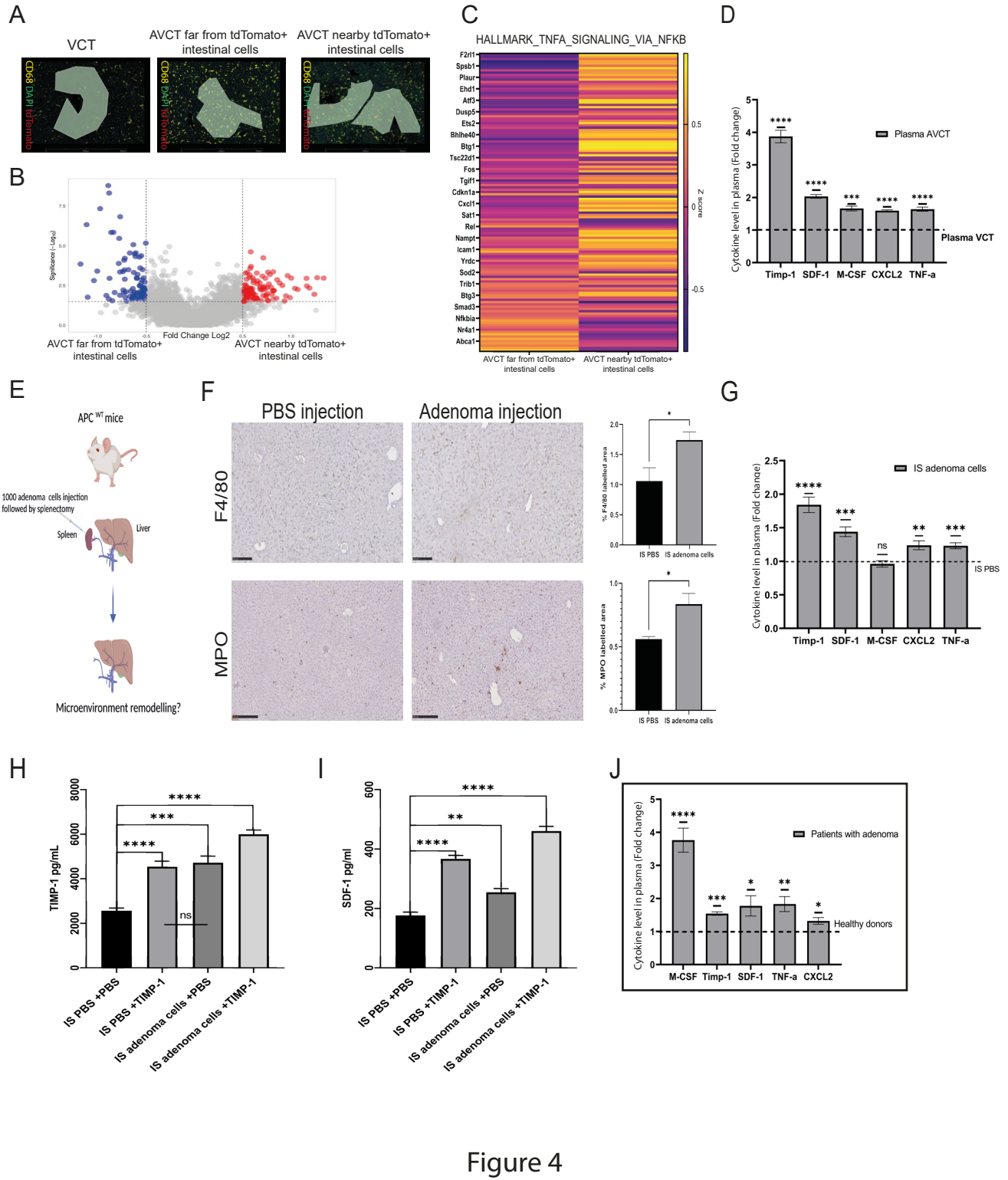

Figure 4

Figure 5

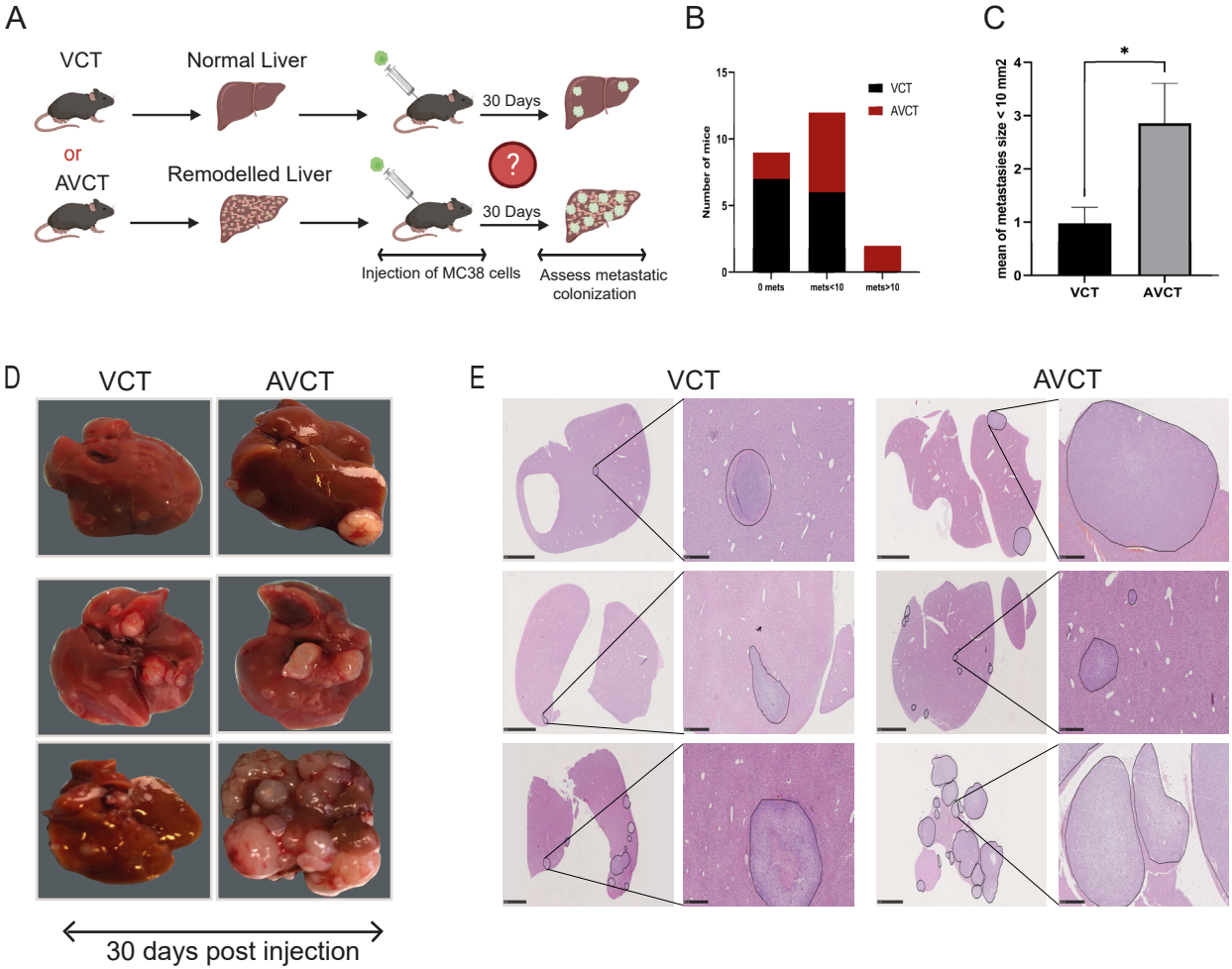

Figure 5

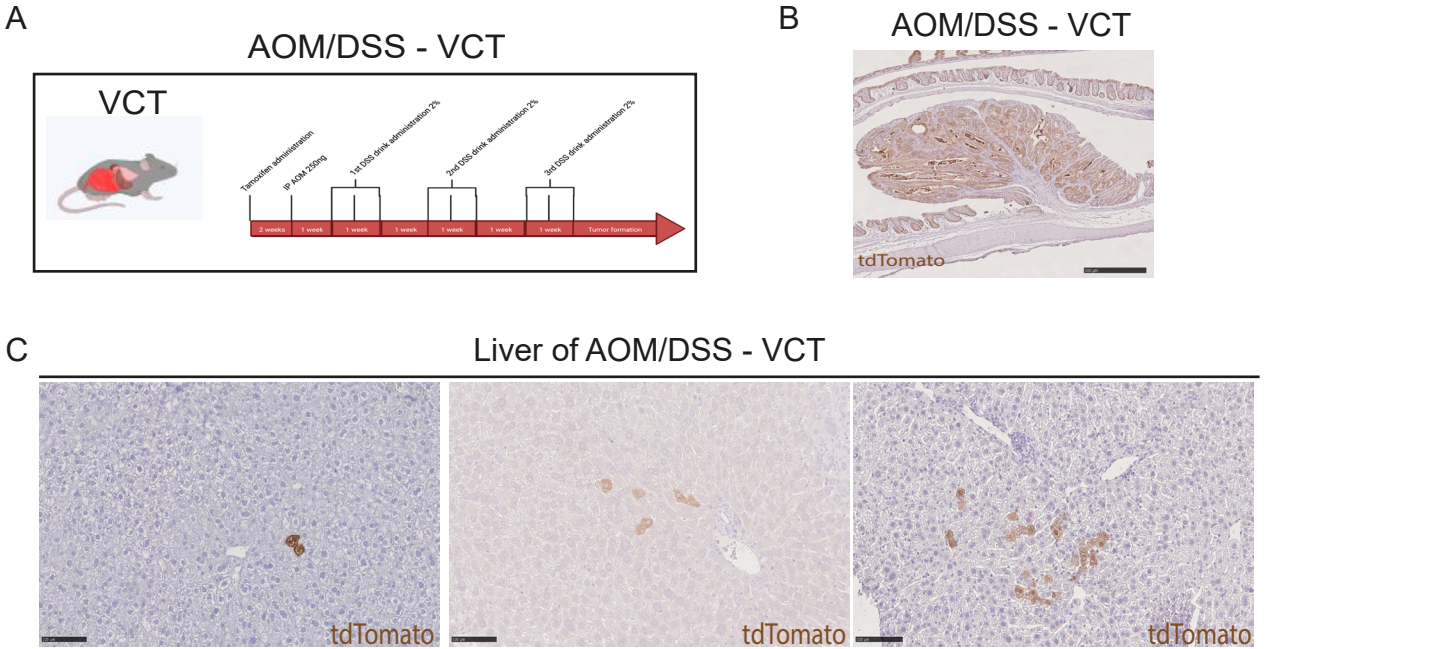

Supplementary Figure S1: **A complementary mouse model for tracking early CRC dissemination**

(A) Schematic description of AOM/DSS protocol applied to tamoxifen-treated VCT mice to induce intestinal tumorigenesis.

(B) Immunohistochemestry using RFP antibody to detect dTomato positive cells on a colonic adenoma and showing a homogenous tdTomato staining validating the mouse model.

(C) Immunohistochemistry using RFP antibody to detect dTomato positive cells on liver sections from 3 different mice with colonic adenomas reveals the presence of rare intestinal tdTomato early-disseminated tumor cells

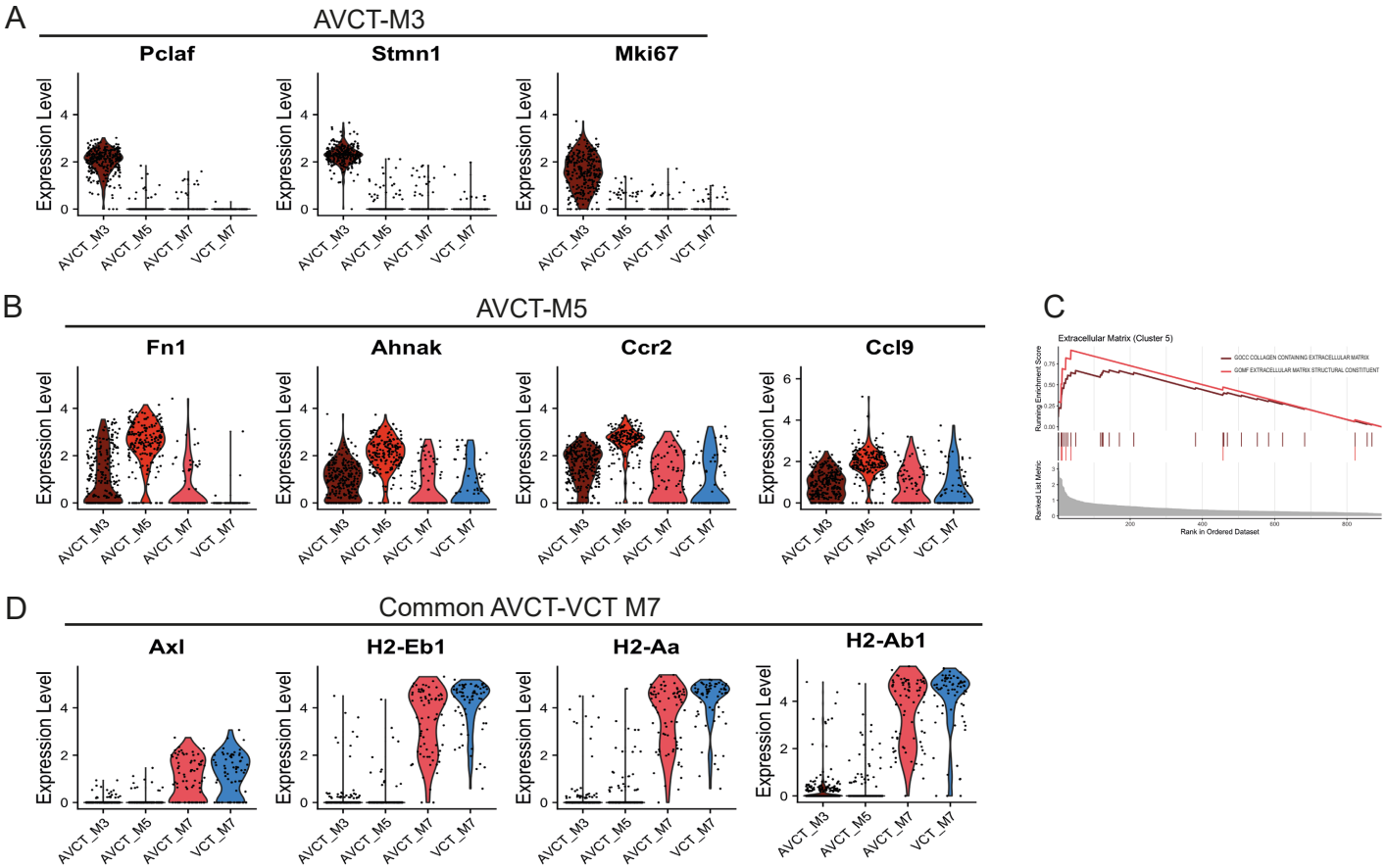

Supplementary Figure S2: **Characterization of macrophages subpopulations in the liver of VCT and AVCT mice**
Violin plots showing the distribution of expression level of the indicated genes across clusters for macrophages cluster M3; M5 and M7 (A, B and D respectively) (see the result part for details)
(C) GSEA plot displaying the enrichment score “ES” of extracellular matrix related GO terms in cluster M5 (P adjust value of GOMF and GOCC 0.0003 and 0.00084 respectively; Enrichment Score of GOMF and GOCC 0.9113 and 0.67426 respectively)

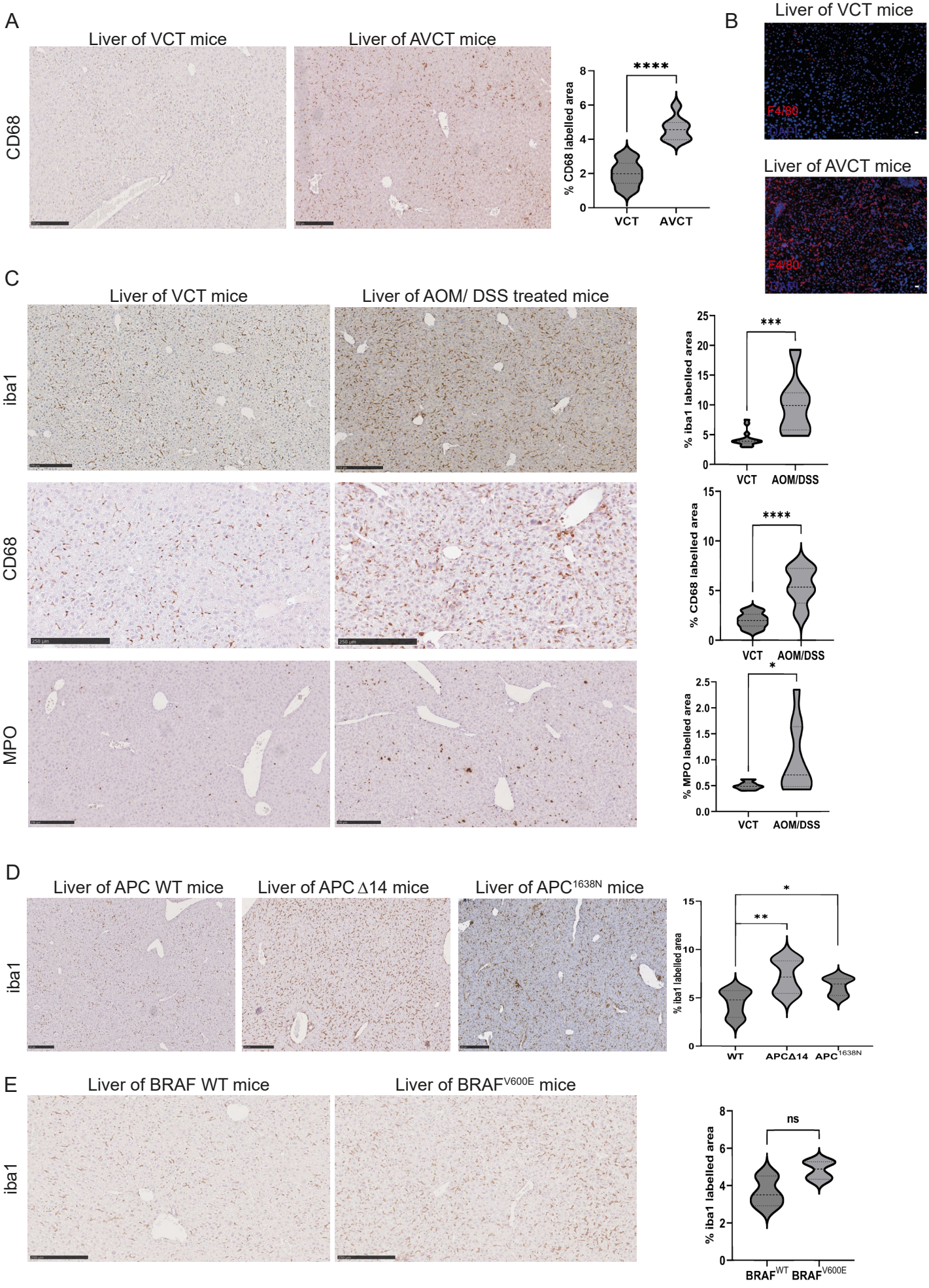

Supplementary Figure S3

Supplementary Figure S3: **Myeloid cell enrichment in complementary mouse models of early intestinal tumorigenesis**

(A) Immunohistochemistry using CD68 antibody to detect macrophages on liver sections from VCT mice (left panel) and AVCT intestinal adenoma bearing mice (middle panel). Right panel shows signal intensity quantification. CD68: n>8, ****p value < 0.0001

(B) Representative image of immunofluorescence using F4-80 antibody to detect macrophages on liver sections from VCT mice (upper panel) and AVCT intestinal adenoma bearing mice (lower panel).

(C) Immunohistochemistry using CD68 and Iba1 antibodies (top and middle panel respectively) to detect macrophages and MPO antibody (bottom panel) on liver sections from AOM and tamoxifen-treated VCT mice bearing colonic adenomas. Right panel shows signal intensity quantifications
iba1: n>7, *** p value = 0.0007 CD68: n>5 **** p value < 0.0001 MPO: n>10 * p value= 0.0235

(D) Immunohistochemistry using Iba1 antibody to stain macrophages on liver sections from APC WT mice (left panel), APCD14 mice (middle panel) and APC1638N mice (right panel). Far right panel shows signal intensity quantifications n=7, ** p value =0.0061 * p value =0.0231

(E) Immunohistochemistry using Iba1 antibody to detect macrophages on liver sections from BRAF WT mice (left panel) and BRAFV600E intestinal adenoma bearing mice (middle panel).
Right panel shows signal intensity quantifications. N=3, p value = 0.0594

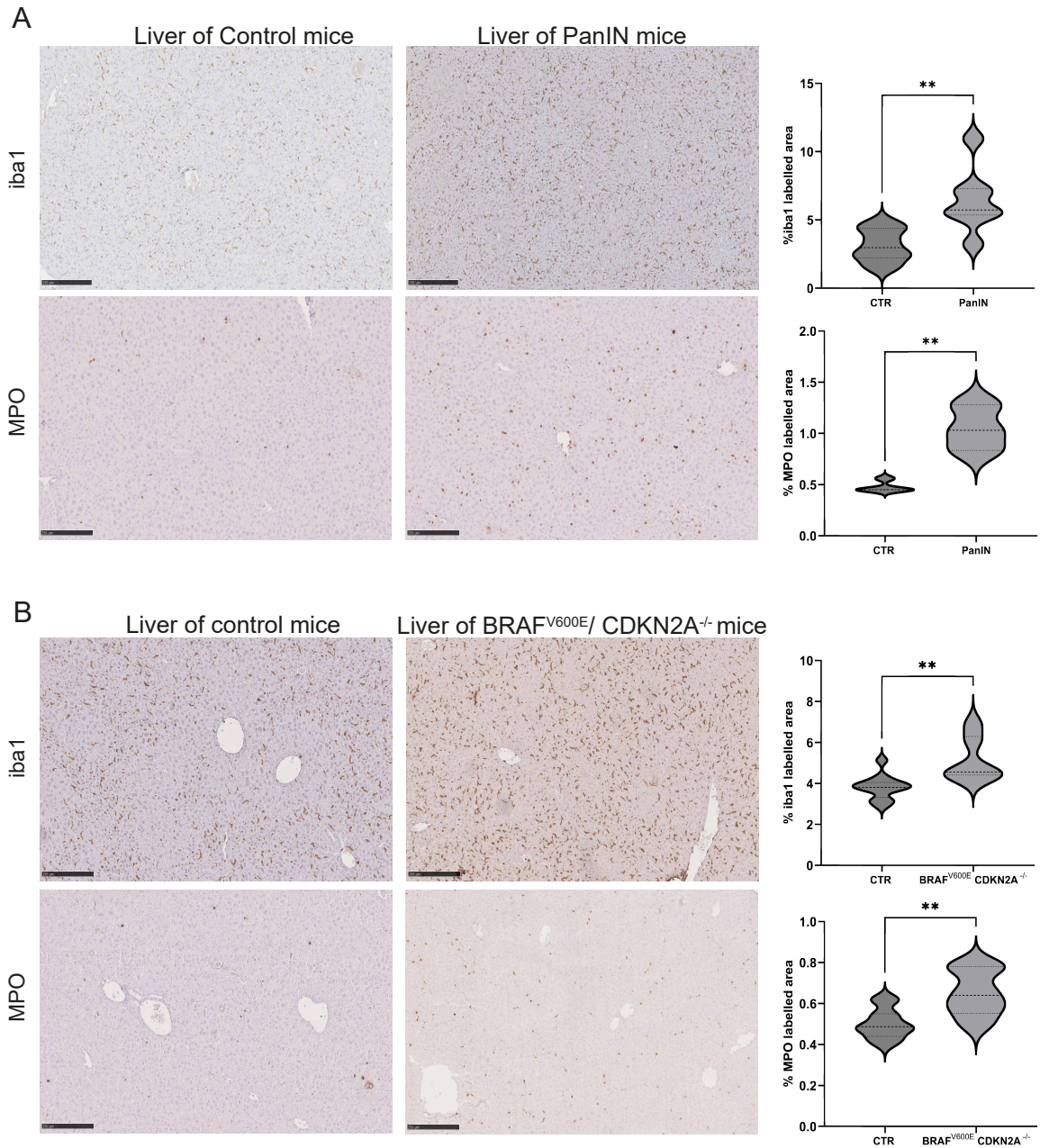

Supplementary Figure S4: **Myeloid cell enrichment in early stages of pancreatic and melanoma mouse models**

(A) Immunohistochemistry using Iba1 antibody (top panel) to detect macrophages and MPO antibody (bottom panel) on liver sections from KPC mice at the PanIN stage (for pancreas cancer). Right panel shows signal intensity quantifications iba1: n>7, ** p value = 0.0018; MPO n>3 ** p value= 0.0039

(B) Immunohistochemistry using Iba1 antibody (top panel) to detect macrophages and MPO antibody (bottom panel) on liver of BRAFV600/CDKN2A-/- mice. Right panel shows signal intensity quantifications iba1: n>6, ** p value = 0.0036 MPO: n>6, ** p value = 0.0043

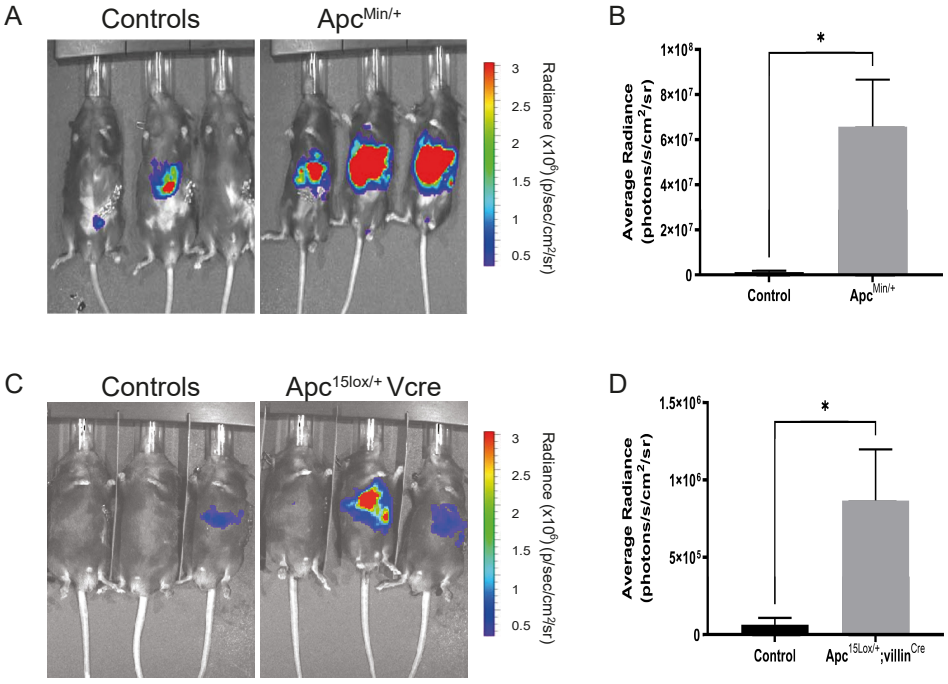

Supplementary Figure S5: **Apc-mutated mice are more susceptible to develop liver metastasis than WT mice**
All animals received intrasplenic injection of 2x106 CMT93-Luc-mCherry cells and bioluminescent signal was acquired by using IVIS invivo imaging system twice a week for 2 weeks.
(A,B) On the left, representative image of bioluminescent signals in the liver at 2 weeks in WT versus ApcMin/+ mice.
On the right, data were shown with the mean radiance ± SEMs of 6 WT and 7 ApcMin/+ mice.
(C,D) On the left, representative image of bioluminescent signals in the liver at 2 weeks in WT versus Apc15Lox/+;Vcre mice.
On the right, data were shown with the mean radiance ± SEMs of 10 WT and 11 Apc15Lox/+;Vcre mice.

Click here to access/download

Supplemental Videos and Spreadsheets

Homayed_Supplemental video 1.mp4

Click here to access/download

Supplemental Videos and Spreadsheets

Homayed_Supplemental video 2.mp4

Click here to access/download

Supplemental Videos and Spreadsheets

Homayed_Supplemental video 3.mp4

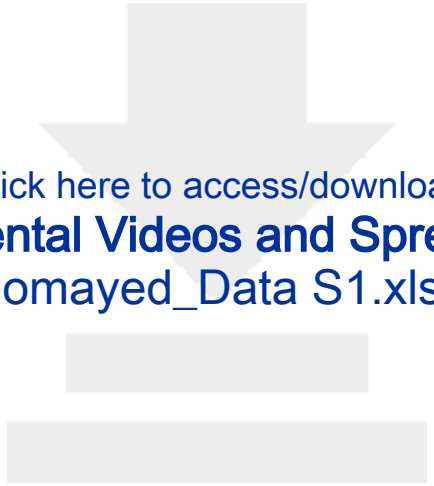

Click here to access/download

Supplemental Videos and Spreadsheets

Homayed_Data S1.xlsx

Click here to access/download

Supplemental Videos and Spreadsheets

Homayed_Data S2.xlsx

CELL PRESS DECLARATION OF INTERESTS POLICY

Transparency is essential for a reader's trust in the scientific process and for the credibility of published articles. At Cell Press, we feel that disclosure of competing interests is a critical aspect of transparency. Therefore, we require a "declaration of interests" section in which all authors disclose any financial or other interests related to the submitted work that (1) could affect or have the perception of affecting the author's objectivity or (2) could influence or have the perception of influencing the content of the article.

What types of articles does this apply to?

We require that you disclose competing interests for all submitted content by completing and submitting the form below. We also require that you include a "declaration of interests" section in the text of all articles even if there are no interests to declare.

What should I disclose?

We require that you and all authors disclose any personal financial interests (e.g., stocks or shares in companies with interests related to the submitted work or consulting fees from companies that could have interests related to the work), professional affiliations, advisory positions, board memberships (including membership on a journal's advisory board when publishing in that journal), or patent holdings that are related to the subject matter of the contribution. As a guideline, you need to declare an interest for (1) any affiliation associated with a payment or financial benefit exceeding $10,000 p.a. or 5% ownership of a company or (2) research funding by a company with related interests. You do not need to disclose diversified mutual funds, 401ks, or investment trusts.

Authors should also disclose relevant financial interests of immediate family members. Cell Press uses the Public Health Service definition of "immediate family member," which includes spouse and dependent children.

Where do I declare competing interests?

Competing interests should be disclosed on this form as well as in a "declaration of interests" section in the manuscript. This section should include financial or other competing interests as well as affiliations that are not included in the author list. Examples of "declaration of interests" language include:

> "AUTHOR is an employee and shareholder of COMPANY."
> "AUTHOR is a founder of COMPANY and a member of its scientific advisory board."

NOTE: Primary affiliations should be included with the author list and do not need to be included in the "declaration of interests" section. Funding sources should be included in the "acknowledgments" section and also do not need to be included in the "declaration of interests" section. (A small number of front-matter article types do not include an "acknowledgments" section. For these articles, reporting of funding sources is not required.)

What if there are no competing interests to declare?

If you have no competing interests to declare, please note that in the "declaration of interests" section with the following wording:

> "The authors declare no competing interests."

CELL PRESS DECLARATION OF INTERESTS FORM

If submitting materials via Editorial Manager, please complete this form and upload with your initial submission. Otherwise, please email as an attachment to the editor handling your manuscript.

Please complete each section of the form and insert any necessary "declaration of interests" statement in the text box at the end of the form. A matching statement should be included in a "declaration of interests" section in the manuscript.

Institutional affiliations

We require that you list the current institutional affiliations of all authors, including academic, corporate, and industrial, on the title page of the manuscript. ***Please select one of the following:***

☒ All affiliations are listed on the title page of the manuscript.

☐ I or other authors have additional affiliations that we have noted in the "declaration of interests" section of the manuscript and on this form below.

Funding sources

We require that you disclose all funding sources for the research described in this work. ***Please confirm the following:***

☒ All funding sources for this study are listed in the "acknowledgments" section of the manuscript.*

*A small number of front-matter article types do not include an "acknowledgments" section. For these, reporting funding sources is not required.

Competing financial interests

We require that authors disclose any financial interests and any such interests of immediate family members, including financial holdings, professional affiliations, advisory positions, board memberships, receipt of consulting fees, etc., that:

(1) could affect or have the perception of affecting the author's objectivity, *or*
(2) could influence or have the perception of influencing the content of the article.

Please select one of the following:

☒ We, the authors and our immediate family members, have no financial interests to declare.

☐ We, the authors, have noted any financial interests in the "declaration of interests" section of the manuscript and on this form below, and we have noted interests of our immediate family members.

Advisory/management and consulting positions

We require that authors disclose any position, be it a member of a board or advisory committee or a paid consultant, that they have been involved with that is related to this study. We also require that members of our journal advisory boards disclose their position when publishing in that journal. ***Please select one of the following:***

☒ We, the authors and our immediate family members, have no positions to declare and are not members of the journal's advisory board.

☐ The authors and/or their immediate family members have management/advisory or consulting relationships noted in the "declaration of interests" section of the manuscript and on this form below.

Patents

We require that you disclose any patents related to this work by any of the authors or their institutions. ***Please select one of the following:***

☒ We, the authors and our immediate family members, have no related patents to declare.

☐ We, the authors, have a patent related to this work, which is noted in the "declaration of interests" section of the manuscript and on this form below, and we have noted the patents of immediate family members.

Please insert any "declaration of interests" statements in this space. This exact text should also be included in the "declaration of interests" section of the manuscript. If no authors have a competing interest, please insert the text, "The authors declare no competing interests."

The authors declare no competing interests

On behalf of all authors, I declare that I have disclosed all competing interests related to this work. If any exist, they have been included in the "declaration of interests" section of the manuscript.

Name: Julie Pannequin

Manuscript number (if available):